A MISSENSE MUTATION IN CONE PHOTORECEPTOR CYCLIC NUCLEOTIDE-GATED CHANNELS ASSOCIATED WITH CANINE DAYLIGHT BLINDNESS OFFERS INSIGHT INTO CHANNEL STRUCTURE AND FUNCTION

A Dissertation
Submitted to
the Temple University Graduate Board

In Partial Fulfillment
of the Requirements for the Degree
DOCTOR OF PHILOSOPHY

---

by
Naoto Tanaka
January, 2014

Examining Committee Members:

Dr. Jacqueline C. Tanaka, Advisory Chair, Biology
Dr. Edward Gruberg, Examining Chair, Biology
Dr. Frank Chang, Biology
Dr. Vincenzo Carnevale, Biology
Dr. Michael O'Leary, External Member, Cooper Medical School of Rowan University

ABSTRACT

Cone cyclic nucleotide-gated (CNG) channels are located in the retinal outer segments, mediating daylight color vision. The channel is a tetramer of A-type (CNGA3) and B-type (CNGB3) subunits. CNGA3 subunits are able to form homotetrameric channels, but CNGB3 exhibits channel function only when co-expressed with CNGA3. Mutations in the genes encoding these cone CNG subunits are associated with achromatopsia, an autosomal recessive genetic disorder which causes incomplete or complete loss of daylight and color vision.

A missense mutation, aspartatic acid (Asp) to asparagine (Asn) at position 262 in the canine CNGB3 subunit (cB3-D262N), results in loss of cone function and therefore daylight blindness, highlighting the crucial role of this aspartic acid residue for proper channel biogenesis and/or function. Asp 262 is located in a conserved region of the second transmembrane segment containing three Asp residues designated the *Tri-Asp motif*. We exploit the conservation of these residues in CNGA3 subunits to examine the motif using a combination of experimental and computational approaches. Mutations of these conserved Asp residues result in a loss of nucleotide-activated currents and mislocalization in heterologous expression. Co-expressing CNGB3 *Tri-Asp* mutants with wild type CNGA3 results in functional channels, however, their electrophysiological characterization matches the properties of homomeric CNGA3 tetramers. This failure to record heteromeric currents implies that Asp/Asn mutations impact negatively both CNGA3 and CNGB3 subunits. A homology model of canine CNGA3 relaxed in a

membrane using molecular dynamics simulations suggests that the *Tri-Asp motif* is involved in non-specific salt bridge pairings with positive residues of S3 – S4. We propose that the CNGB3-D262N mutation in daylight blind dogs results in the loss of these interactions and leads to an alteration of the electrostatic equilibrium in the S1 – S4 bundle. Because residues analogous to *Tri-Asp* residues in the voltage-gated Shaker K^+ channel superfamily were implicated in monomer folding, we hypothesize that destabilizing these electrostatic interactions might impair the monomer folding state in D262N mutant CNG channels during biogenesis.

Another missesnse sense mutation, Arginine (Arg) to tryptophan (Trp) at position 424 in the canine CNGA3 subunit (cA3-R424W), also results in loss of cone function. An amino acid sequence alignment with Shaker K^+ channel superfamily indicates that this R424 residue is located in the C-terminal end of the sixth transmembrane segment. A3-R424W mutant channels resulted in no cyclic nucleotide-activated currents and mislocalization with intracellular aggregates. However, the localization of cA3-R424W mutant channels was not affected as severely as the Asp/Asn mutation in S2 *Tri-Asp motif*, showing a lot of cells with the proper localization of Golgi-like and membrane fluorescence. Moreover, the substitution of Arg 424 to Lysine (Lys), conserving the positive charge, preserved channel function in some cells, which is different from the results of the S2 *Tri-Asp* motif in which the Asp/Glu substitutions, conserving the negative charge, leads to loss of cyclic nucleotide-activated currents. Even though these missense mutations are both associated with canine daylight blindness, the Arg 424 residue might not be as critical for folding as the *Tri-Asp* residues in the S2 *Tri-Asp motif*

and might be more of a problem in channel structure and function. The cA3 model relaxed with MD simulations indicated a possible interaction of Arg 424 with the Glu 304 residue in the S4-S5 linker. This hypothesis is supported by electrophysiological data in which the double mutation of reversing these residues, Glu 306 to Arg and Arg 424 to Glu (E306R-R424E) preserves channel function. In the model, this salt bridge appears to contribute to stabilization of the open pore state. The R424W mutation might disrupt the salt bridge formation, leading to deforming and closing the pore region.

I would like to dedicate this dissertation to my PI, Dr. Tanaka,

who has been always there for me during this journey

even when I was the worst version of myself.

ACKNOWLEDGMENTS

First, I would like to thank My PI, Dr. Jacqueline C. Tanaka. I have never argued with anyone as much as with her in my entire life. Despite all of our differences, it all worked out in a very interesting and wonderful way. I also would like to thank Dr. Edward Gruberg for having encouraged me to be in the program and being supportive of me through the program. Being a TA for his mammalian physiology was definitely one of the highlights in my graduate school. Enzo, I cannot describe how grateful I am to you for introducing me to this amazing world of computational science. You have broadened my horizon and have completely changed my perspective in science. Lucie, there is no word to express my appreciation and gratitude for all of your support and mentoring. You are not just the greatest teacher but also my new best friend. It has been a pleasure to collaborate with Dr. Komáromy, and his clinical aspects have definitely enriched our research. Ama and Asli, thank you so much for being such great lab mates and for assistance with experimental techniques.

All investigations conformed to the ARVO statement for the Use of Animals in Ophthalmic and Vision Research and were approved by the University of Pennsylvania Institutional Animal Care and Use Committee (protocol number (803429; Institutional NIH/PHS Animal Welfare Assurance number A3079-01).

This work was supported by the National Institutes of Health-National Eye Institute (R01-EY019304) and by the National Science Foundation through major research instrumentation grant number CNS-09-58854. LD receives funding from the European Union Framework Program (PIOF-GA-2012-329534) “Voltsens”.

TABLE OF CONTENTS

Page

LIST OF TABLES

LIST OF FIGURES

CHAPTER 1

INTRODUCTION

1.1 Cyclic Nucleotide-Gated Channels

Cyclic nucleotide-gated (CNG^i) channels in retinal rod and cone outer segments mediate dim light vision and daylight color vision, respectively. These channels are activated by the binding of intracellular cyclic guanosine monophosphate (cGMP) whose levels are regulated by a photon-activated biochemical cascade (Yau and Hardie, 2009). In the dark, cGMP levels are the highest, ~ 1 - 5 μM. When CNG channels open, cations flow into the cell down the electrochemical gradient. This inward current depolarizes the cell. In the light, on the other hand, a photon activates Rhodopsin (Rh) in the membrane disc of rods (cone opsin in cones). The activated Rhodopsin (Rh*) activates the G-protein transducein (Gt), catalyzing GDP-GTP exchange on the α-subunit of G-protein transducin (Gtα). The activated α-subunit of G-protein transducin (Gtα*) activates Phosphodiesterase (PDE), which hydrolyzes cGMP to GMP. The cGMP levels decrease and more CNG channels are closed, hyperpolarizing the cell. CNG channels regulate the influx of both Na^+ and Ca^{2+} into the outer segment; Na^+ is the major current carrying ion while Ca^{2+} is an important signal molecule involved in regulating the kinetics of recovery and adaptation. In photoreceptors, cyclic adenosine monophosphate (cAMP) is a weak agonist, yet its physiological role is unknown.

CNG channels are also located in the cilia, thin protrusions, of the dendritic end of olfactory receptor neurons (ORNs) in the main olfactory epithelium for sensory

transduction (Biel and Michalakis, 2009). In ORNs, cAMP is the main ligand to open CNG channels. Olfactory CNG channels regulate the flux of mainly Ca^{2+} and little Na^{+}. This Ca^{2+} influx depolarizes the cell as well as activates physiological cascade pathways, and opens Cl^{-} channels. CNG channels have been identified in non-sensory tissues, such as brain, kidney, or sperm, yet little information is available pertaining to their function or subunit composition (Kaupp and Seifert, 2002; Kraus-Friedmann, 2000).

1.2 CNG channel architecture

CNG channels are non voltage-gated members of the tetrameric Shaker potassium (K^{+}) channel superfamily. A CNG channel is composed of A-type and B-type subunits. Each subunit has 6 transmembrane-spanning helices: a pore-forming region formed by the assembly of S5 and S6 and four auxiliary domains spanning S1 – S4 (Yu et al., 2005), corresponding to vestigial voltage-sensing domains. The intracellular N-terminal regions of CNG channels are involved in trafficking with C-termini (Shuart et al., 2011; Trudeau and Zagotta, 2002a) and contain regulatory sites specific to the channel function (Grunwald et al., 1998; Peng et al., 2003a; Trudeau and Zagotta, 2002b; Trudeau and Zagotta, 2003). The C-terminal region of CNG channels is located on the cytoplasmic side and contains a C-linker between the S6 helix and the cGMP binding domain (Zong et al., 1998). A-type subunits contain a C-terminal leucine zipper (CLZ) domain involved in subunit assembly, whose trimeric coil-coiled structure has been solved by X-ray crystallography (Shuart et al., 2011; Zhong et al., 2003). Indeed, CNG channels are

heteromeric assemblies. Specifically, cone CNG channels consist in a heterotetrameric assembly of CNGA3 (A3) and CNGB3 (B3) subunits.

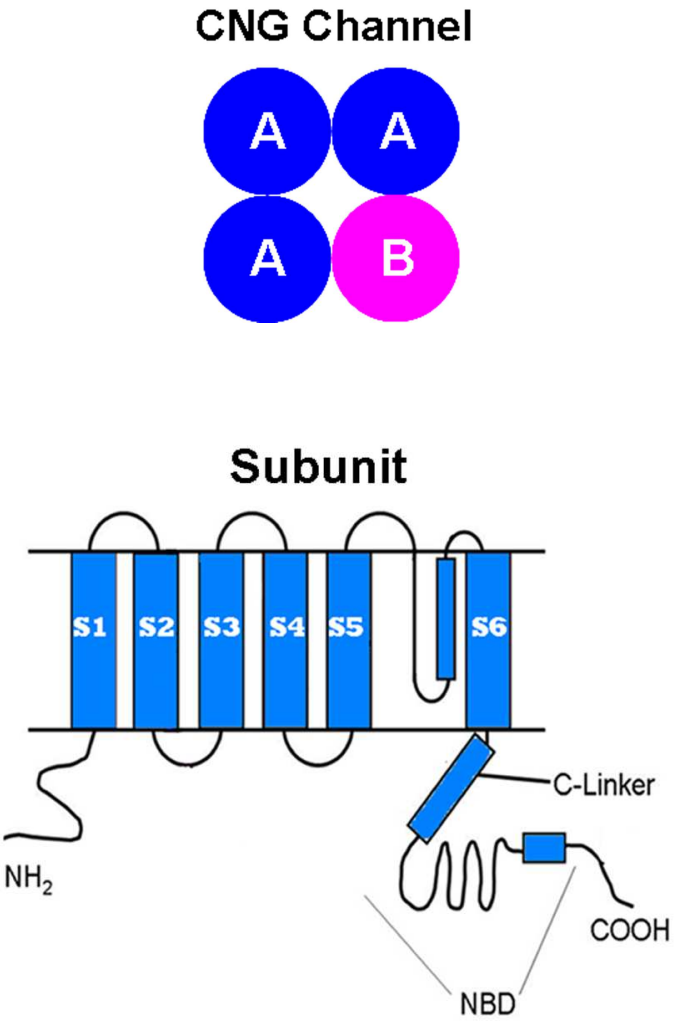

Figure 1.1 Schematics of a CNG channel (top) and a single subunit (Bottom). A CNG channel is composed of A-type and B-type subunits. Each subunit has 6 transmembrane segments, S1 – S6.

1.3 Assembly of CNG channel subunits

The stoichiometry of cone channels is still debated (Peng et al., 2004; Shuart et al., 2011; Zhong et al., 2003), while the rod channel stoichiometry has been firmly established at 3:1 CNGA1:CNGB1 (A1:B1) as in Figure 1.2 (Weitz et al., 2002; Zheng et al., 2002; Zhong et al., 2002). According to previous studies (Shuart et al., 2011; Zhong et al., 2003), tetramerization occurs in two sequential steps. First, three A-type subunits trimerize through the interaction between their CLZ domains. In a second step, a fourth subunit will assemble with the preformed trimmer to generate a tetramer. If a B-type subunit is available, it is preferred over an A-type subunit (Peng et al., 2004; Shuart et al., 2011; Zhong et al., 2003). CNG channels in olfactory receptor neurons are composed of two kinds of A-type subunits (A1 and A2) and one B-type subunit (B1), with a stoichiometry of 1: 2: 1, respectively (Zheng and Zagotta, 2004).

So far, 4 A-type and 2 B-type subunits have been identified in the CNG channel family. A1 – A3 form functional homomeric channels, but A4, B1, and B3 are functional only with co-expression of A1 – A3 (Kaupp and Seifert, 2002). Each homomeric or heteromeric channel has distinct $K_{0.5}$ and efficacy values for cGMP and cAMP (see CHAPTER 2 for detail).

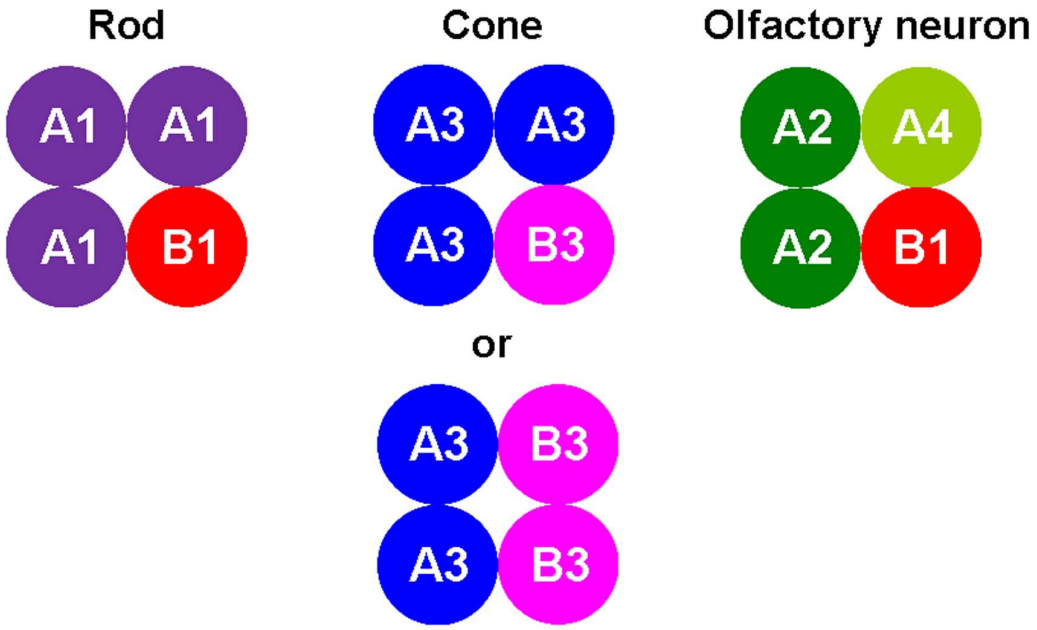

Figure 1.2 Schematics of CNG channel stoichiometry. The rod CNG channel is composed of three A1 + one B1 subunits. The stoichiometry of A3 and B3 subunits in the cone CNG channel is 3:1 or 2:2. The olfactory neuron consists of two A2, one A4, and one B1 subunits.

1.4 Missense mutation and channelopathy

A great deal of autosomal recessive genetic disorders are known to be caused by a single amino acid change, but how does a single amino acid mutation in a channel cause a disease? The most well-known genetic channel disease, "channelopathy," is Cystic Fibrosis (CF) (O'Sullivan and Freedman, 2009). The common symptoms are viscous secretions and clogged airways in the lungs caused by abnormal transport of Cl and Na ions. The most common CF is associated with a deletion of Phe (F) 508 in cystic fibrosis transmembrane conductance regulator (CFTR), a chloride channel. Another inherited channelopathy is long QT syndrome associated with missense mutations, such as Thr (T)

474 to Ile (I), Ala (A) 614 to Val (V), or Val (V) 630 to Leu (L), in the human Ether-a-go-go-Related Gene (hERG) channel (Nakajima et al., 1998). Each of these missense mutations can cause prolonged ventricular repolarization, leading to arrhythmia and sudden death.

1.5 Achromatopsia

Mutations in the genes encoding cone CNG channel subunits, ~ 80 in *A3* and ~ 40 in *B3*, are associated with human achromatopsia. This autosomal recessive channelopathy results in incomplete or complete loss of cone function (Kohl et al., 1993; Kohl et al., 1998; Sundin et al., 2000; Thiadens et al., 2009; Xu et al., 2013). The disease is characterized by poor visual acuity, lack of color discrimination, photophobia, and pendular nystagmus. This phenotype has been attributed to defects in CNG channel subunit folding and assembly, cellular localization and/or channel function (Ding et al., 2010; Matveev et al., 2010; Patel et al., 2005; Saliba et al., 2002).

In Pingelap, the Island of the Colorblind coined by the neurologist Oliver Sachs, 10% of the ~3,000 people living there are affected by, and ~30% are carriers of a missense mutation, Ser (S) 435 to Phe (F), in the *CNGB3* gene (Kohl et al., 2000; Sundin et al., 2000). The most frequently occurring achromatopsia mutation is a missense mutation of Arg (R) 283 to Trp (W) in human (h) A3 (Muraki-Oda et al., 2007).

Achromatopsia is also caused by mutations in other genes as well. Mutations in cone *GNAT2* encoding the α-subunit of cone transducin G protein (Aligianis et al., 2002;

Kohl et al., 2002) and *PDE6C*, encoding the cGMP phodiesterase α-subunit (Ouechtati et al., 2011) have been associated with achromatopsia.

1.6 Canine achromatopsia models

An achromatopsia-like disease was identified in dogs exhibiting daylight blindness and a loss of cone ERG function (Komaromy et al., 2010; Sidjanin et al., 2002). Breeding the progeny of affected dogs resulted in two colonies of affected dogs whose cone loss of function was associated with mutations in the *B3* gene. A German Shorthair Pointer colony inherited a missense mutation of Asp (D) 262 to Asn (N) in the B3 subunit and an Alaskan Malamute mutation resulted in a deletion of the B3 subunit (Figure 1.3) (Sidjanin et al., 2002). Recently, another missense mutation, Arg (R) 424 to (Trp) W, was identified in the *A3* gene of German Shorthair Pointer dogs (publication in progress). The identification of canine mutations in the *A3* and *B3* genes provide a new model for investigating achromatopsia as well as the structure and function of cone CNG channels.

Figure 1.3 Canine models for achromatopsia in German shorthaired pointer (left) and Alaskan Malamute (right) dogs. A missense mutation D262N in the *cB3* gene (German), a missense mutation R424W in the *cA3* gene (German), a deletion of the *cB3* gene (Alaskan) result in the same clinical phenotype as human patients with complete Achromatopsia. The pictures are from http://www.petguide.com/breeds/dog/german-shorthaired-pointer and http://en.wikipedia.org/wiki/File:Alaskan_Malamute.jpg, respectively.

1.7 Gene replacement therapy with canine achromatopsia models

Gene replacement therapy has been explored to treat genetic diseases, and retinal inherited disorders are good models with relatively high success rates in animals and humans (Komaromy et al., 2010). Dr. Aguirre, Dr. Komáromy, and colleagues have been performing gene replacement therapy to treat daylight blind *B3* mutant dogs (Komaromy et al., 2010). Since the *cB3* gene has not been cloned yet, *hB3* has been substituted in the therapy. The effect of the treatment is age-dependent with a higher success rate in younger dogs; the restoration of cone function lasted up to 2 years. In order to reduce the chance of immunological inflammatory responses and to make the effect of the therapy longer, efforts are underway to clone the *cB3* gene for treatment. The day-blind mutant

dogs provide a model closely-related to the human eye for investigating inherited retina diseases as well as therapeutic advances.

CHAPTER 2

ELECTROPHYSIOLOGICAL CHARACTERIZATION OF CANINE CNGA3

2.1 Introduction

2.1.1 Why have cone CNG channels been studied less than rod CNG channels?

The elegant and thorough biochemistry and physiology on vertebrate rods has not been replicated on cones because rods dominate most vertebrate retinas and rods tend to be larger than cones. Early work on catfish cones by Haynes defined the CNG channel activation and electrophysiological properties (Haynes and Yau, 1985; Haynes and Yau, 1990; Haynes, 1995). More recently, Korenbrot and collaborators contributed significantly to our understanding of cone physiology using striped bass cones (Korenbrot, 1995; Korenbrot, 2012; Paillart et al., 2006). The cone properties were later matched to those of heterologously-expressed channels once the genes were available for study. Since the first CNG channel gene, *A1*, was cloned from bovine retinal rods in 1989 (Kaupp et al., 1989), rod CNG genes have been cloned form more than 8 retinas of different species, including human and canine (Richards and Gordon, 2000), and studied for over two decades. In contrast, cone CNG channel genes, *A3* and *B3*, have been cloned and investigated to a lesser extent (Biel and Michalakis, 2009).

2.1.2 Distinct electrophysiological properties of CNG channels

Within the CNG channel family, channels from rod, cone and olfactory neurons exhibit identifiable activation, conductance and pharmacological properties (Kaupp and

Seifert, 2002). In heterologous expression systems using either *Xenopus* oocytes or eukaryotic cells in culture, CNG channels are distinguished by characteristic cGMP- and cAMP-activation, block by L-*cis*-diltiazem, and ion selectivity (Biel and Michalakis, 2009). Since B-type subunits do not form functional channels without an A-type subunit, B-type subunit properties are inferred by comparing homomeric and heteromeric channel properties.

In photoreceptor CNG channels, cyclic guanosine monophosphate (cGMP) is the main ligand, while cyclic adenosine monophosphate (cAMP) is a weak agonist (Kaupp and Seifert, 2002). The cGMP (or cAMP) dose response curve of each CNG channel exhibits a distinct $K_{0.5}$ value, the concentration at which the current is half-maximal. The ratio of the maximum cAMP current to the maximum cGMP current at saturating concentrations is commonly known as the cAMP efficacy. This cAMP efficacy varies depending on the subunit composition of a CNG channel. $K_{0.5}$ and cAMP efficacy values are typically used as fingerprints of CNG channel subunit compositions, yet the physiological role of cAMP is unknown.

Diltiazem, a benzothiazepine, is a Ca^{2+} channel antagonist which binds to and blocks the pore-forming region of the channel (Abernethy and Schwartz, 1999; Levine et al., 2013). Diltiazem is used as a drug for hypertension, cardiac arrhythmia, migraine, and bipolar disorders (Abernethy and Schwartz, 1999). An isomer of diltiazem, L-*cis*-diltiazem, is known to bind to B-type subunits of CNG channels and block heteromeric channel currents and little homomeric currents (Liu et al., 2013; Peng et al., 2003b; Peng et al., 2004; Shuart et al., 2011). One electrophygiological study suggests that the

binding site for L-*cis*-diltiazem might be in the pore region of a B-type subunit (Shuart et al., 2011), yet the biochemical details of diltiazem blocking are to be determined. Although the pharmacological relevancy of L-*cis*-diltiazem blocking in CNG channels is unknown, these properties are used to distinguish between homo- and heteromeric channels.

CNG channels are non-selective cation channels for both monovalent and divalent ions, yet the permeability of each ion is different (Kaupp and Seifert, 2002; Wells and Tanaka, 1997). In rod cells, the relative permeabilities of physiologically relevant cations are determine as $Ca^{2+} > Na^{+} \sim K^{+} > Mg^{2+}$ (Wells and Tanaka, 1997). The divalent ions, Ca^{2+} and Mg^{2+}, not only permeate but also block CNG channels by binding to and staying in the pore region of the channel (Kaupp and Seifert, 2002; Wells and Tanaka, 1997). Since Ca^{2+} is known to play many important roles in the retinal outer segments for light adaptation through a complex set of Ca^{2+}-induced reactions, the permeability and blocking properties of Ca^{2+} in CNG channels have been studied (Kaupp and Seifert, 2002; Wells and Tanaka, 1997; Yau and Hardie, 2009). When rod (A1), olfactory neuron (A2,) or cone (A3) homomeric channels are heterologously expressed, each shows a distinct Ca^{2+} permeation property (Frings et al., 1995). Moreover, A1 homo- and A1 + B1 heteromeric rod channels show distinct properties in voltage-dependent Ca^{2+} blockage; A1 homomeric cGMP-activated currents are blocked more by Ca^{2+} than A1 + B1 heteromeric currents due to the existence of the glutamic acid-rich protein (GARP) in the N-terminus of the B1 subunit (Korschen et al., 1995). Given that CNG channels are known to provide a Ca^{2+} entry pathway for physiological cascades such as light

adaptation (Kaupp and Seifert, 2002), these distinct Ca^{2+} related properties of CNG channels might be important to maintain the proper balance of the intracellular Ca^{2+} concentration in each cell type.

Our collaborator Dr. Komáromy and colleagues successfully cloned the *A3* gene from canine retinal tissues for the first time as submitted at GenBank (BankIt1673058 cCNGA3 KF806731). Our laboratory was asked to investigate the electrophysiological properties of cone CNG channels expressing canine (c) *A3* in a heterologous expression system. We characterized the cGMP- and cAMP-activated currents, voltage-dependent L-*cis*-diltiazem blocking, dose responses, and Ca^{2+} permeation. Since canine *B3* gene is not available, human *B3* gen was substituted to examine heteromeric channel properties (refer to 2.1.4 for detail).

2.1.3 Cloning of *canine CNGA3*

Canine *A3* (*cA3*) gene was cloned from intact retinas and total RNA was isolated from the retinal tissue in the Komáromy lab. First strand cDNA was synthesized by PCR using forward and reverse primers; two pair of *cA3* specific primers were designed to amplify the coding region of the gene. The full-length gene was cloned into pCR-TOPO-II® (Invitrogen) and sequenced. The *cA3* sequence is determined and available from GenBank (BankIt1673058 cCNGA3 KF806731.

The *cA3* gene was then sub-cloned into a yellow fluorescent protein (YFP) expressing vector, pEYFP-N1® (Clonetech), in the Tanaka lab (Figure 2.1). The *cA3* gene was restricted from the pCR-TOPO-II® vector using BamHI (New England

BioLabs) and EcoRI (New England BioLabs) restriction endonucleases. In order to introduce HindIII restriction site at the 5' end of the gene and AgeI restriction site at the 3'end of the gene in a way the stop would be eliminated, PCR was performed using Pfu turbo® DNA Polymerase (Agilent) and a pair of primers as follows:

5'- CGGAAGCTTGCAGAGATGGCCAAGATTAACACCCAAGTCTCC-3' and;

5'-GGCGACCGGTGACTGCTCTTTGATCTCTGTTTTTGCGGC-3'.

The pEYFP-N1 vector was restricted by HindIII and AgeI restriction endonucleases, and the PCR gene product was ligated into the pEYFP using T4 DNA Ligase (Promega). The ligation product, *cA3-Y*, was transformed into E coli cells, Library Efficiency® DH5α Competent Cells (Invitrogen), by heat shock. The transformed cells were grown in S.O.C medium (Invitrogen) for one hour and plated on LB agar-plated (10g tryptone, 5g yeast extract, and 10g NaOH in 1L H_2O plus 15g agar) with 50 μg/ml kanamycin overnight. A colony was picked and grown in 5ml LB medium (10g tryptone, 5g yeast extract, and 10g NaOH in 1L H_2O) with 50 μg/ml kanamycin in a shaker at 37 °C for 5 -7 hours. Approximately, 100 μl of the culture was used to inoculate 100 ml LB medium with 50 μg/ml kanamycin overnight. The *cA3* gene in the pEYFP-N1 vector was extracted using QIAGEN Plasmid Midi Kit (QIAGEN), and the full length gene was sequenced and confirmed using a set of sequence primers designed as in Table 2.1

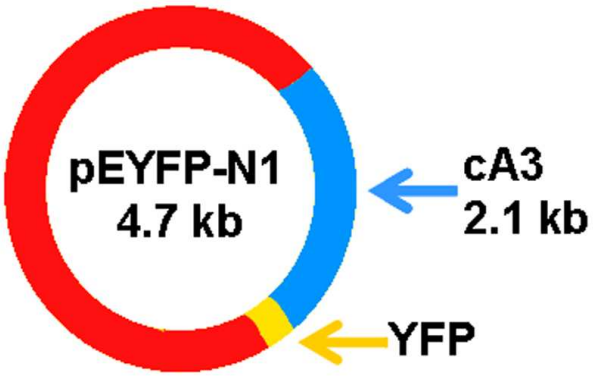

Figure 2.1 Schematic of the *cA3* gene inserted in the pEYFP-N1 vector. The *cA3* gene is 2.1 kb, and the vector is 4.7 kb, which makes the total length 6.8 kb. YFP is located after replacing the stop site of the gene at the C-terminus. c = canine. YFP = yellow fluorescent protein.

Table 2.1 Sequencing primers for the *cA3* gene. A set of primers were designed to sequence the full length of each gene. The antisense prime reads the sequence on the antisense. c = canine.

Gene	Sequencing primer (SP)	Primer sequence (5' – 3')
cA3	cA3-SP-606 (antisense)	GCACACCAGCAGACACCAG
	cA3-SP1-397	AGAAACAACAACAACAACTG
	cA3-SP2-1154	CCCCTGTAAAAGATGAGGAGTACGTG

2.1.4 Attempts to clone canine *CNGB3* and substitution of human *CNGB3*

Although the sequence of the *cB3* gene was previously reported (Sidjanin et al., 2002), attempts to clone the gene into a eukaryotic expression vector have been unsuccessful to date. I wanted to investigate the pathophysiology of the *cB3* missense mutation and our collaborator wanted to use the *cB3* gene for gene replacement therapy to treat daylight blind dogs. Despite the fact that we spent almost a year on this project,

we were unable to clone the full-length gene without numerous mutations. The problem seemed to be at nucleotide encoding Gly (G) 374 which resulted in an unintended stop mutation. The PCR product had the wild-type sequence as confirmed by sequencing, however after transformation, the same mutation would reappear. We used multiple E.coli strains for transformation including Library Efficiency® DH5α Competent Cells (Invitrogen), XL1-Blue (Agilent) and One Shot® Chemically Competent E.coli (Life Technology), yet none worked. Since *cB3* is a eukaryotic gene, we considered cloning using yeast, but our lab is not equipped to do this procedure. After all, we decided to abort the project and to use human *B3* (*hB3*) gene which had been successfully used for gene replacement therapy and restores sight in daylight blind dogs.

The *hB3* gene was a gift from Bernd Wissinger. The gene was cloned into pCDNA 3.1™ (Invitrogen) for eukaryotic expression. The *hB3* gene was inserted into pEYFP-C1 or pEYFP-N1 to examine the cellular localization of the fluorescent tag, yet it led to the failure of heteromeric channel expression when co-expressed with untagged cA3. For this reason, all heteromeric channel studies were comprised of *cA3* in pEYFP co-expressed with *hB3* in pcDNA3.1.

Table 2.2 Sequencing primers for the canine *CNGB3* gene. A set of primers were designed to sequence the full length of each gene. The antisense prime reads the sequence on the antisense. c = canine.

Gene	Sequencing primer (SP)	Primer sequence (5' – 3')
cB3	cB3-SP-891 (antisense)	GGCATTACTGACGCAACATCC
	cB3-SP1-694	CCACTACGCCTCGTCTTTCC
	cB3-SP2-1530	CCTCAGCATCATCAGCAAAGTCG

2.2 Materials and methods

2.2.1 Amino acid sequence alignments of canine and human A3 and B3 subunits

Amino acid sequences of cA3 (GI: 345777245), hA3 (GI: 4502917), cB3 (GI: 50978664), and hB3 subunit (GI: 116642889) were aligned using Clustal X version 2.0.1. (Larkin et al., 2007) (http://www.clustal.org/). The blocks of amino acid substitution matrix were used, together with standard parameters (opening gap penalty of 10, gap extension penalty of 0.20, and gap distance of 5). The major domains were then assigned according to the previous studies (Brelidze et al., 2012; Long et al., 2007; Shuart et al., 2011): the N-terminus, the transmembrane region (S1 – S6), C-linker, and cyclic nucleotide binding domain (CNBD), plus the C-terminal leucine zipper (CLZ) domain for A subunits (refer to Figure 2.2).

2.2.2 Heterologous expression

1) Cell culture medium

The cell culture medium was made of Dulbecco's Modified Eagle's Medium (DMEM) – high glucose (Sigma), 1.85 g of Sodium Bicarbonate ($NaHCO_3$), and 10 % of Fetal Bovine Serum (FBS), Premium (Sigma). 6.7 g of DMEM and 1.85 g of $NaHCO_3$ were dissolved in 500 ml of H_2O, and the pH was adjusted to 7.2. Then, 50 ml of fetal bovine serum was added in a sterile environment.

2) Cell culture

The human embryonic kidney (HEK) cell line tSA201 was used for expression studies. These cells were kept in 1 ml FBS and 10% Dimethyl Sulfoxide (DMSO) (Sigma) at - 80 °C. A 1 ml vial of cells was raised in 10 ml of the culture medium and grown at 37 °C for 24 hours. The grown cells were washed with 5 ml of Phosphate-Buffered Saline (PBS), composed of 137 mM NaCL, 2.7 mM KCl, 10 mM Na_2HPO_4, and 1.8 mM KH_2PO_4. Two ml of 0.05% Trypsin-EDTA (Gibco) was added to dissociate the cells. The cells were triturated in 5 ml of the culture medium and centrifuged for 3 minutes. The media was discarded, and the cells were raised in 1 ml of fresh medium. The number of cells in 1 ml was counted using a hemocytometer , and ~ 200,000 cells were added and grown on coverslips in a 2 ml of the culture medium at 37 °C for 24 hours.

3) Transfection

The cells were transfected employing Lipofectamine™ 2000 (Invitrogen) as published previously (Patel et al., 2005). Ten µl of Lipofectamine was added in 250 ml of the serum free culture medium (6.7 g of DMEM and 1.85 g of $NaHCO_3$ in 500 ml of H_2O). Separately, 2 - 3 µg of the *cA3-Y* gene or 1 - 2 µg of the *cA3-Y* gene and 2 - 4 µg the *hB3* gene were added in 250 ml of the serum free culture medium. After 5 minutes, these two Lipofectamine and gene containing solutions were mixed and sat for 30 minutes. The culture medium of the grown cells from previous day was changed, and the

Lipofectamine and gene mix was added in the fresh culture medium. After transfection procedure, the cells were grown at 37 °C for 24 hours.

2.2.3 Electrophysiology

1) cGMP- and cAMP-activated current recordings

Inside-out patches were performed on transfected cells using glass electrodes with resistances of 1.2 - 4.2 MΩ, in a bath solution containing 120 mM NaCl, 2 mM EDTA, 2 mM EGTA, and 5 mM Hepes at pH 7.4. Concentrations of cGMP in the range of 1 – 500 µM and cAMP in the range of 100 – 10000 µM, were added to the bath. A series of 300-ms voltage pulses were applied in 10-mV steps between - 80 mV and 80 mV. Currents were recorded at room temperature with an amplifier (AXOPATCH 10) and digitizer (DIGIDATA 1322A) and were analyzed on computer software (Clampfit 10.0™, Table curve™, Sigmaplot™). The net currents were obtained by subtracting the bath current from each cAMP or cGMP activated current. Current data were averaged from multiple traces and fitted by the Hill equation, $I = I_{max} / [1 + (K_{0.5} / L)^{Nh}]$. For L-cis-diltiazem and $K_{0.5}$ values, net currents were normalized to the maximum cGMP activated current for each patch.

2) Ca^{2+} reversal potential shift recordings

For Ca^{2+} reversal potential (E_{Rev}) measurements, the bath solution was 120 mM NaCl and 5 mM Hepes at pH 7.4 with 1 mM Ca^{2+} added to the bath in the presence and absence of cGMP. A voltage ramp was applied from -20 mV to +20 mV and back to -20

mV. The currents with ascending and descending ramps were digitally averaged and linearized to obtain a best fit to the zero current value or E_{Rev} (Wells and Tanaka, 1997). The relative permeability ratio of calcium to sodium, P_{Ca}/P_{Na}, after single-sided addition of Ca^{2+}, was determined according to the Goldman-Hodgkin-Katz current equation extended to include E_{Rev} permeant divalent cations and ignoring surface charge effects. The ratio can then be determined using the Lewis equation (Lewis, 1979) as follows:

$$P_{Ca}/P_{Na} = \{\{[Na]_o - ([Na]_i e^{FErev/RT})\}(1+e^{FErev/RT})\} / \{4([Ca]_i \cdot e^{2FErev/RT} - [Ca]_o)\}.$$

2.3 Results

2.3.1 Amino acid sequence alignment of canine and human CNGA3 and CNGB3

1) Canine and human CNGA3 subunits

The amino acid sequence of cA3 is aligned with that of hA3 using Clustal X version 2.0.1. (Larkin et al., 2007) (http://www.clustal.org) as in Figure 2.2. According to the previous studies (Brelidze et al., 2012; Long et al., 2007; Shuart et al., 2011), domains are assigned as the N-terminus, the transmembrane region (S1 - S6), C-linker, cyclic nucleotide binding domain (CNBD), and the C-terminal leucine zipper (CLZ) domain. The cA3 subunit is highly homologous with the hA3 subunit, the amino acid sequence identity is determined to be 82% by blastp (protein-protein BLAST) (http://blast.ncbi.nlm.nih.gov). Most of the sequence variation between canine and human A-type subunits resides in the N-terminus as two gaps.

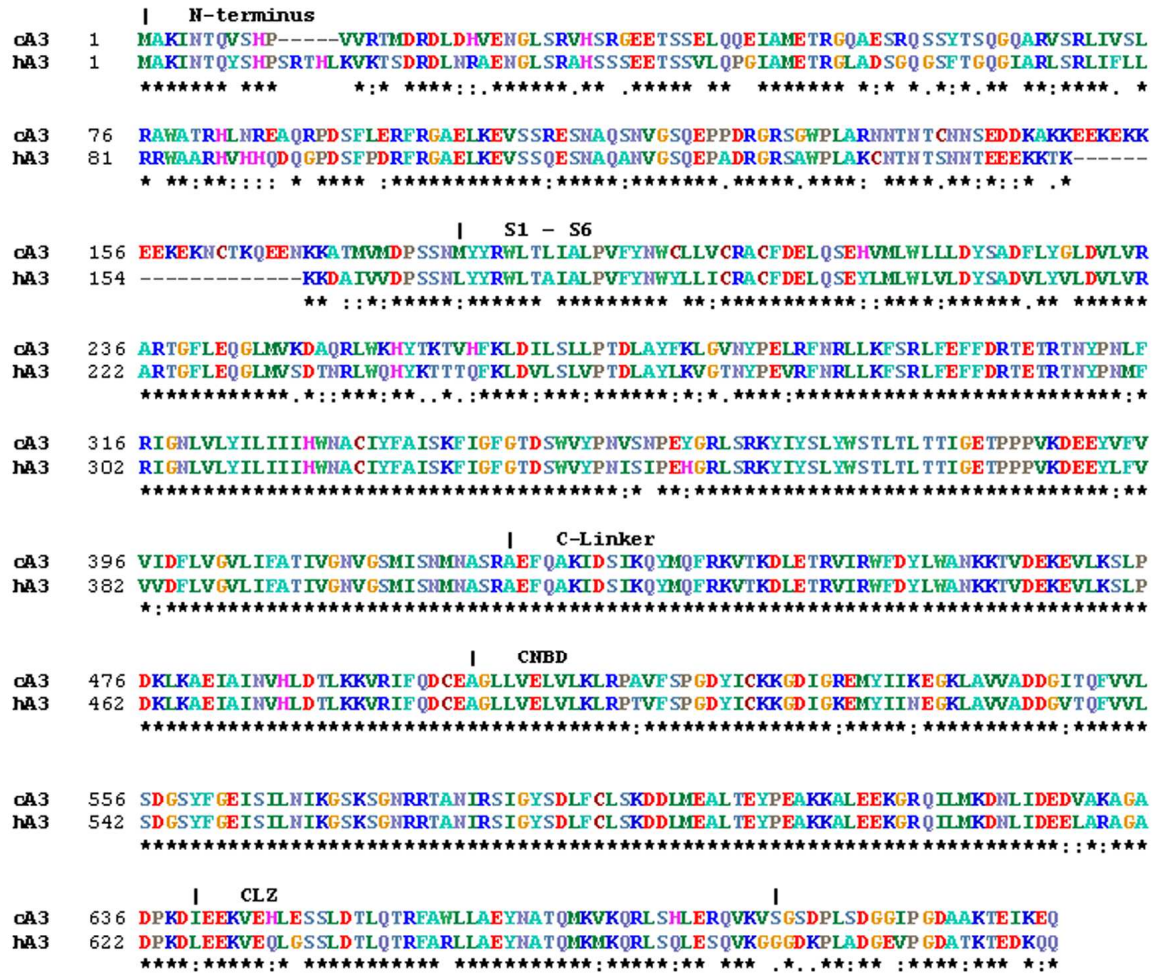

Figure 2.2 Amino acid sequence alignment of canine CNGA3 and human CNGA3. The amino acid sequence identity between the cA3 and hA3 is 82%. The stars indicate sharing the same amino acid, two vertical dots mean sharing similar chemical properties, and one dot indicates belonging in the same amino acid group. Each domain is assigned according to the previous studies (Brelidze et al., 2012; Long et al., 2007; Shuart et al., 2011). c = canine, h = human. S1 – S6 = transmembrane region, CNBD = cyclic nucleotide binding domain, CLZ = C-terminal leucine zipper domain.

2) Canine and human CNGB3 subunits

The amino acid sequence of cB3 is aligned with that of hB3 using Clustal X version 2.0.1. (Larkin et al., 2007) (http://www.clustal.org) as in Figure 2.3. Major domains (S1 - S6, C-linker, and CNBD) are assigned according to the previous studies (Brelidze et al., 2012; Long et al., 2007; Shuart et al., 2011). The cB3 and hB3 subunits are highly homologous with the amino acid sequence identity of 76% (protein-protein BLAST) (http://blast.ncbi.nlm.nih.gov), which explains the reason that *hB3* is consistent with the successfully substitution of the human for the canine *B3* for gene replacement therapy in daylight blind dogs. Most of the sequence variation (not aligned here) between A-type and B-type subunits resides in the C-leucine zipper (CLZ) domain involved in the trimerization of the A-type subunits of CNG channel (Shuart et al., 2011; Zhong et al., 2002).

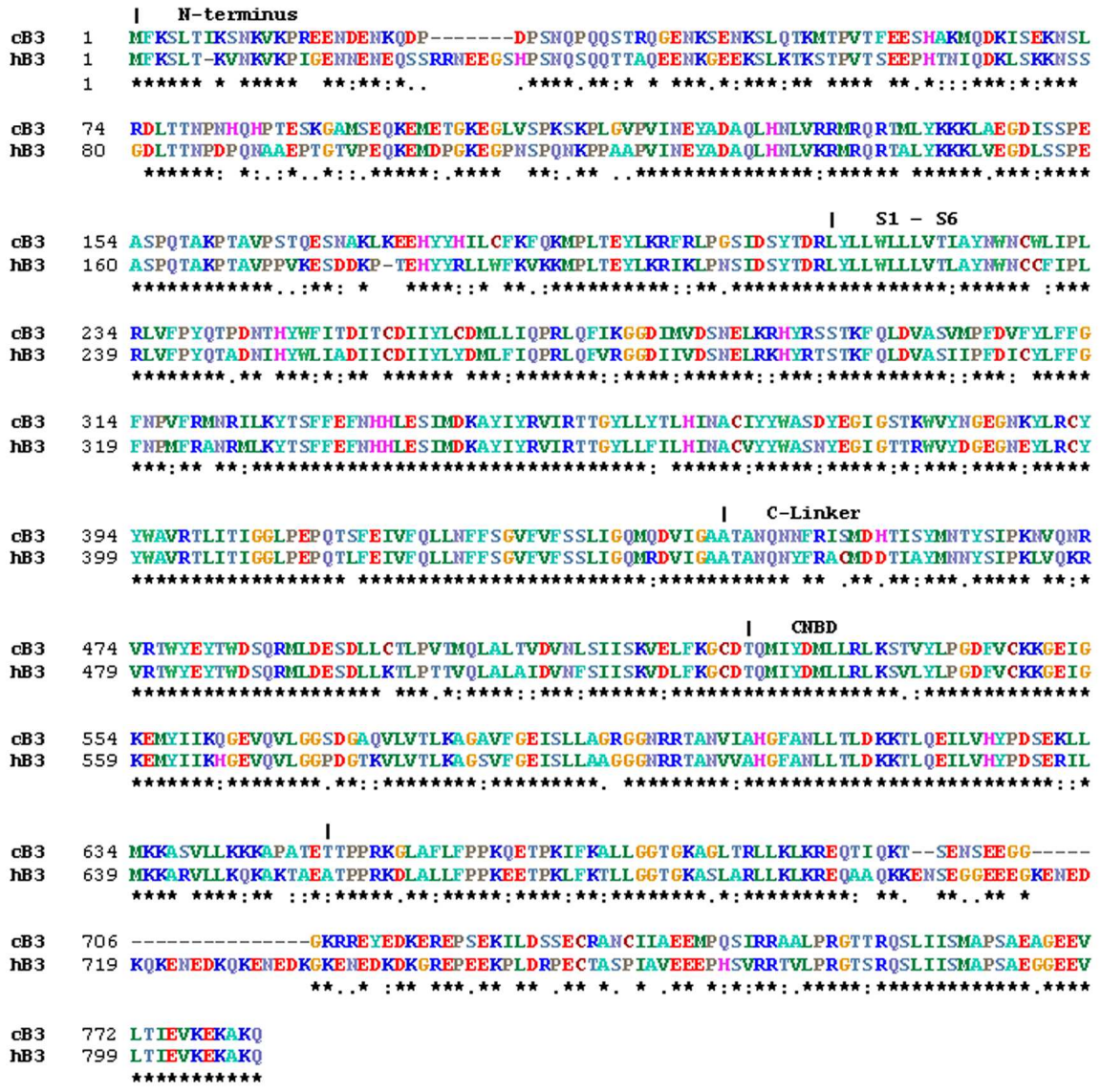

Figure 2.3 Amino acid sequence alignment of canine CNGB3 and human CNGB3. The amino acid sequence identity between the cB3 and hB3 is 76%. The notation for this alignment is identical to the previous figure.

2.3.2 Electrophysiological properties of homomeric canine CNGA3 and heteromeric canine CNGA3 + human CNGB3 channels

1) cGMP and cAMP activated currents

Patch clamp electrophysiology was used to examine the function of CNG channels expressed in tSA201 cells. Inside-out patches were excised from cells expressing homomeric cA3 or heteromeric channels co-expressing cA3 plus hB3. Figure 2.4 shows a representative patch with nucleotide activation of homomeric (left) and heteromeric channels (right). Channels were activated with saturating concentrations of 200 μM cGMP and 5 mM cAMP; the net currents were determined by subtracting the bath current from the nucleotide-activated current. Relative to the maximum cGMP-activated current at saturating concentrations, the maximum cAMP-activated current of homomeric channels is smaller than that of hetromeric channels. The ratio of the cAMP activated current of homomeric channels to the cGMP current of hetromeric channels for this patch is 0.14, whereas the ratio is 0.38 for the hetromeric. On average, the efficacy of cAMP to cGMP elicited about 19% of the maximal cGMP-activated current from homomeric channels and about 33% from heteromeric channels. Co-expression of hB3 with cA3 results in an increase of the cAMP current, and an increase in the cAMP efficacy serves as a fingerprint for heteromeric channels. The results from multiple experiments are shown in Table 2.3

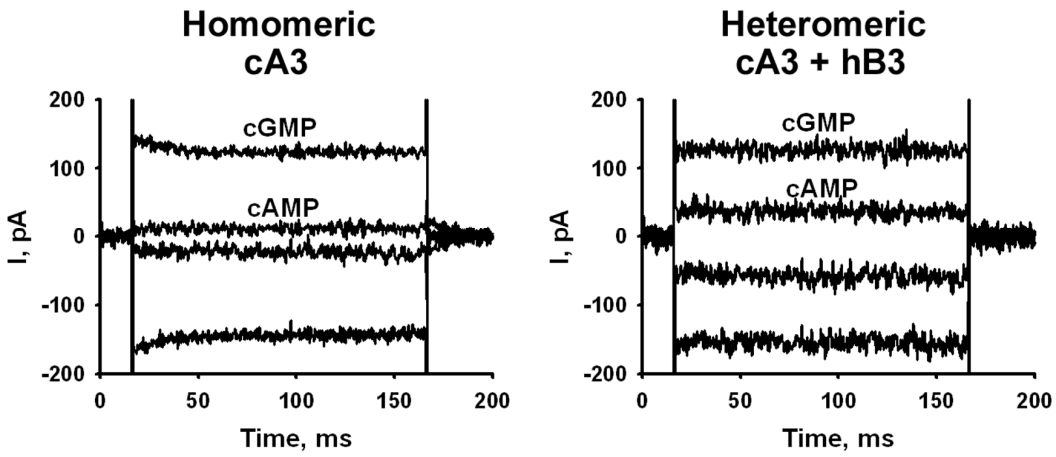

Figure 2.4 Nucleotide-activated currents from homomeric canine CNGA3 (left) and hetromeric canine CNGA3 and human CNGB3 (right) channels. Each panel shows the net currents of homomeric (left) or hetromeric (right) channels with 5000 μM cAMP and 200 μM cGMP at -60 mV and 60 mV. Currents were activated with 200 μM cGMP and 5000 μM cAMP at -60 mV (negative currents) and 60 mV (positive currents). The cAMP efficacy is 0.14 for homomeric channels and 0.38 for hetromeric channels.

2) IV curves with cGMP and cAMP activation and with L-*cis* diltiazem block

Representative current-voltage (*I-V*) relations at saturating concentrations of cGMP and cAMP are shown in Figure 2.5 for homomeric cA3 in panel A (left) and heteromeric cA3 + hB3 channels in panel A (right). A slight inward rectification is seen with both channel types as shown by the larger inward (negative) currents. This property is seen with both cGMP and cAMP activation. The inward rectification at 60 mV is 1.6 fold for cGMP and 2.2 fold for cAMP. A similar pattern is seen for hetromeric channels with 1.25 fold rectification for cGMP and 1.7 fold for cAMP. Panel B shows representative IV relations activated by 100 μM cGMP and 25 μM L-*cis* diltiazem in 100 μM cGMP for homomeric cA3 and heteromeric cA3 + hB3 channels respectively. The

diltiazem block on the homomeric is 10% at -60 mV, whereas it is 70% for the hetromeric. Diltiazem blocking provides another assay to distinguish between homomeric and heteromeric CNG channels. The results from multiple experiments are summarized in Table 2.3.

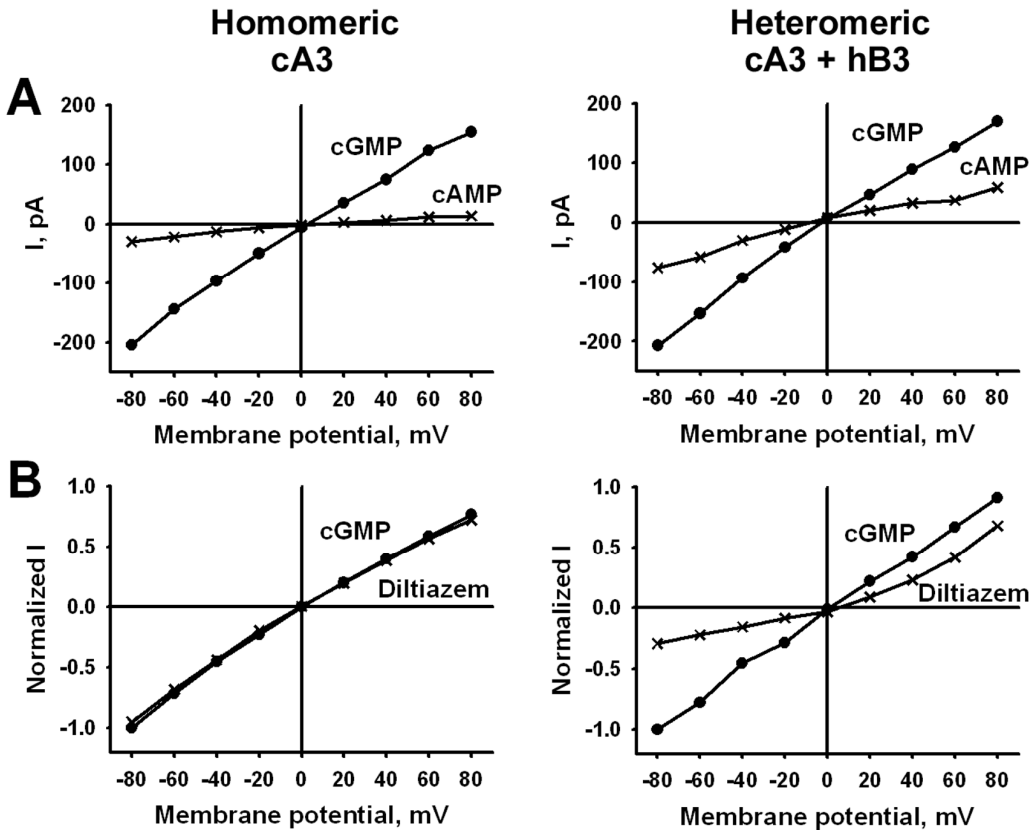

Figure 2.5 (A) Cyclic nucleotide-activated IVs from homomeric ccnine CNGA3 (upper left) and heteromeric canine CNGA3 + human CNGB3 (upper right). Both the electrode and bath solutions have EDTA and EGTA to eliminate the characteristic Ca^{2+} block of Na^{+} current in CNG channels. In the absence of divalent cations, a slight inward rectification is observed with a 1.6 fold larger current at -60 mV compared to 60 mV for cGMP and 2.2 fold for cAMP in homomeric channels. Little change is seen in heteromeric channels containing the human B3 subunit with rectification of 1.25 fold for cGMP and 1.7 fold for cAMP.
(B) L-*cis* Diltiazem current block IVs from homomeric canine CNGA3 (lower left) and heteromeric canine CNGA3 + human CNGB3 (lower right). IVs were recorded with 100 μM cGMP alone or with 25 μM L-*cis*-diltiazem added to the bath. The net currents were normalized to the maximum cGMP activated current for each patch.

3) cGMP and cAMP dose-response relationships

Figure 2.6 shows a dose-response relationship of CNG channels with cGMP and cAMP activation for homomeric (left) and heteromeric (right) channels. The $K_{0.5}$ value

for cGMP increases from 14.4 to 18.4 µM with co-expression of the B3 subunit; the $K_{0.5}$ values for cAMP are near 1 mM for both channel types. Averaged results from multiple patches are shown in the table and compared with results from human CNG channels. The average canine $K_{0.5}$ value for cGMP is 10.3 µM, between 8.6 and 13.5 µM for hA3 homomeric channels. Similarly, canine CNGA3 $K_{0.5}$ values of 16 µM for co-transfected cA3 with hB3 fall close to values measured for hA3 heteromeric channels of 18.2 and 19.9 µM. The consistent feature seen for cone channels is that co-expression with the B3 subunit shifts the $K_{0.5}$ to higher values. Since the cB3 subunit has not yet been cloned, this shift may reflect the property of the hB3 subunit used in our experiments. However, the overall function of the cA3 channel closely reflects that of the hA3 channels.

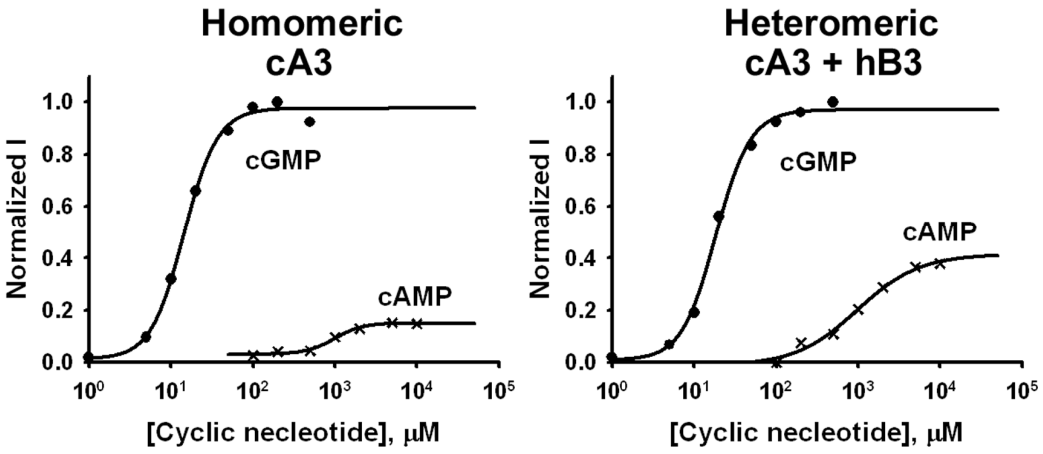

Figure 2.6 cAMP and cGMP dose response relationships of homomeric canine CNGA3, (left) and heteromeric canine CNGA3 + human CNGB3, (right) channels. Each plot shows the ligand concentration-dependent activation of homomeric (left) or heteromeric (right) channels at - 60 mV. Data for each channel type were taken from a single patch. Data were taken from a single patch. The $K_{0.5}$ for cGMP is 14.2 µM for homomeric and 18.6 µM for heteromeric channels; the N_h is 2.1 for both channel types. The cAMP $K_{0.5}$ values are 947 µM and 966 µM, respectively with N_h values of ~ 2.5.

4) Reversal potentials of cGMP-activated currents in presence of 1 mM Ca^{2+} provide a measure of Ca^{2+} permeation and voltage-dependence of block.

Figure 2.7 shows representative current-voltage (*I-V*) relations of CNG channels with 200 μM cGMP activation in presence or absence of 1 mM intracellular Ca^{2+}. When patching with Ca^{2+} the reversal potential (V_{rev}) shifts to more negative values for both homomeric (left) and heteromeric (right) channels as compared to V_{rev} without calcium. The V_{rev} of the cA3 + hB3 heteromeric channel has a greater negative shift than that cA3 homomeric channel, - 0.47 and - 4.02. respectively. The permeability ratio of calcium to sodium, P_{Ca}/P_{Na}, of the homomeric channel is 1.56, whereas that of the heteromeric channel is 15.16. The data from multiple patches are shown in Table 2.3.

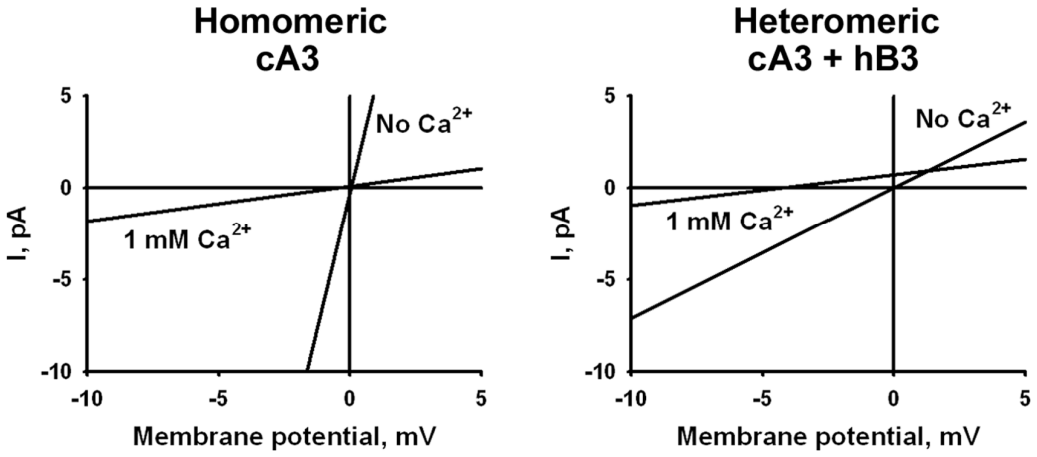

Figure 2.7 Current reversal potential shifts (E_{rev}) in the presence or absence of 1 mM $[Ca^{2+}]_i$ with 200 μM cGMP. Each panel shows net currents activated by 200 μM cGMP with and without 1 mM calcium. Voltage ramps were -20 V to 20 V. The E_{rev} shift of homomeric channels is - 0.47 mV, whereas that of the heteromeric is - 4.02 mV.

Table 2.3 Comparison of canine CNG channel function to human CNG channels. The $K_{0.5}$ values, Hill coefficients (N_h), cAMP efficacy (I_{cAMP} / I_{cGMP}), and L-*cis* diltiazem block (I_{dil} / I) of homomeric and hetromeric channels were determined at -60 mV. Averaged Ca^{2+} permeability was 1.52 ± 0.52 (n = 5) for cA3 and 17.7 ± 6.4 for cA3 + hB3 (n = 4). Comparison values on hA3 were not available. c = canine, h = human.

cGMP		**cAMP**		**I_{cAMP} / I_{cGMP}**	**I_{dil} / I**	**References**
$K_{0.5}$ (µM)	**N_h**	**$K_{0.5}$ (µM)**	**N_h**			
			cA3			
10.3 ± 1.24 (7)	2.40 ± 0.33	1665 ± 226 (7)	2.06 ± 0.30	0.19 ± 0.01 (16)	0.79 ± 0.05 (4)	This work
			hA3			
13.5 ± 2.5 (39)	2.2 ± 0.2	1329 ± 3.69 (39)	1.3 ± 0.2	0.12 ± 0.04 (39)	0.94 ± 0.04 (6)	Peng, 2003 a
12.9 ± 0.5 (62)	2.1	1212 ± 37 (53)	1.4	0.12 ± 0.01 (48)		Peng, 2003 b
8.20 ± 0.34 (7)	1.90 ± 0.13	580 ± 110 (10)	1.39 ± 0.37			Koeppen, 2008
11.1 ± 1.0 (13)	1.83 ± 0.19					Okada, 2004
8.63 ± 0.8 (21)	1.53 ± 0.17					Reuter, 2008
			cA3 + hB3			
16.0 ± 1.05 (6)	1.87 ± 0.15	1569 ± 262 (6)	2.36 ± 0.66	0.33 ± 0.02 (25)	0.40 ± 0.02 (8)	This work
			hA3 + hB3			
19.9 ± 3.8 (56)	2.0 ± 0.2	897 ± 1.77 (56)	1.6 ± 0.2	0.27 ± 0.09 (59)	0.26 ± 0.11(15)	Peng, 2003 a
15.8 ± 0.3 (61)	2.0 ± 0.2	846 ± 33 (54)	1.5 ± 0.3	0.36 ± 0.01 (48)		Peng, 2003 b
19.4 ± 1.6 (6)	1.65 ± 0.18	570 ± 60 (6)	1.03 ± 0.13			Koeppen, 2008
26.2 ± 1.9 (16)	1.82 ± 0.11					Okada, 2004
18.2 ± 1.8 (13)	1.22 ± 0.15					Reuter, 2008

2.4 Summary

2.4.1 Canine CNGA3 channels showed similar elctrophysiological properties to human CNGA3 channels.

Here we described the electrophysiological properties of the cA3 channel and compare the characteristics with previously published data from the human channel (Koeppen et al., 2008; Okada et al., 2004; Peng et al., 2003a; Peng et al., 2003b; Reuter et al., 2008). The weak cAMP efficacy and weak L-*cis* diltiazem block of the A3 homomeric channel match previous work as shown in Table 1. Co-expression of cA3 with hB3 results in an increase in cAMP efficacy and an increase in L-*cis* diltiazem block. The average cGMP $K_{0.5}$ value for cA3 homomeric channels is 10.3 µM, which falls between 8.6 and 13.5 µM reported for hA3 channels. Similarly, the somewhat higher $K_{0.5}$ value of 16 µM cGMP in cells expressing cA3 and hB3 is close to values measured for hA3 + hB3 of 18.2 and 19.9 µM. The cAMP $K_{0.5}$ values are more difficult to obtain because of the small currents and there is a wide variation in previous data. One finding of potential physiological relevance to intracellular Ca^{2+} levels in cone outer segments not previously reported is the relative permeability of Ca^{2+} to Na^{+}. Interestingly, we find that the P_{Ca}/P_{Na} is increased ~10 fold when the B3 subunit is co-expressed with A3, which suggests that alterations in Ca^{2+} homeostasis could be associated with the *cB3* daylight blind mutations and could be responsible for the loss of cone function (refer to CHAPTER 6 DISCUSSION).

CHAPTER 3

CANINE DAYLIGHT BLIND MISSENSE MUTATION, *CNGB3-D262N*, IN A HIGLY CONSERVED S2 *TRI-ASP MOTIF*

3.1 Introduction

3.1.1 Canine *CNGB3-D262N* misesense mutation in a highly conserved acidic region of S2: *Tri-Asp motif*

In a canine achromatopsia model, loss of cone ERG function and daylight vision are associated with the mutation of Asp (D) 262 to Asn (N) in the B3 subunit. This daylight blind missense mutation suggests an important role for Asp 262 in cone function. In analogy to Shaker K^+ channels, D262 of the cB3 is located at the C-terminal end of the 2nd transmembrane segment (S2) (denoted as D3 in Figure 3.1). N-terminal to D3, there are two other Asp residues, D252 and D256 (denoted as D1 and D2 respectively). This short region with three aspartic acid residues is highly conserved amongst CNG channels and extending to some related Shaker superfamily channels; therefore, I designated this region as the *Tri-Asp motif*. Human Ether-a-go-go-Related Gene (hERG) channels conserve the *Tri-Asp* motif, and hyperpolarization-activated cyclic nucleotide (HCN) channels contain Asp residues at D2 and D3 positions. Other Kv channels conserve acidic residues at the flanking positions, D1 and D3. The evolutionary conservation highlights the universal role of the *Tir-Asp motif*.

In order to investigate the molecular properties of the missense mutation, I exploited the conservation of the *Tri-Asp motif* and the propensity of A3 subunit to

express functional homomeric channels. I generated a cA3-D3/N (mutating the conserved Asp 231 residue in the cA3 subunit) mutant subunit and a D3/N mutation in *hB3 (hB3-D267N*). I further asked whether conservation of the negative charge substituting aspartic acid (D) with glutamic acid (E) could preserve channel function. Similarly, whether the other Asp residues in the in the highly conserved *Tri-Asp motif* could tolerate substitutions. To investigate further the *Tri-Asp motif*, I generated canine and human A3 mutant subunits with nonpolar, polar, and, and charged amino acids as in Materials and methods and Results.

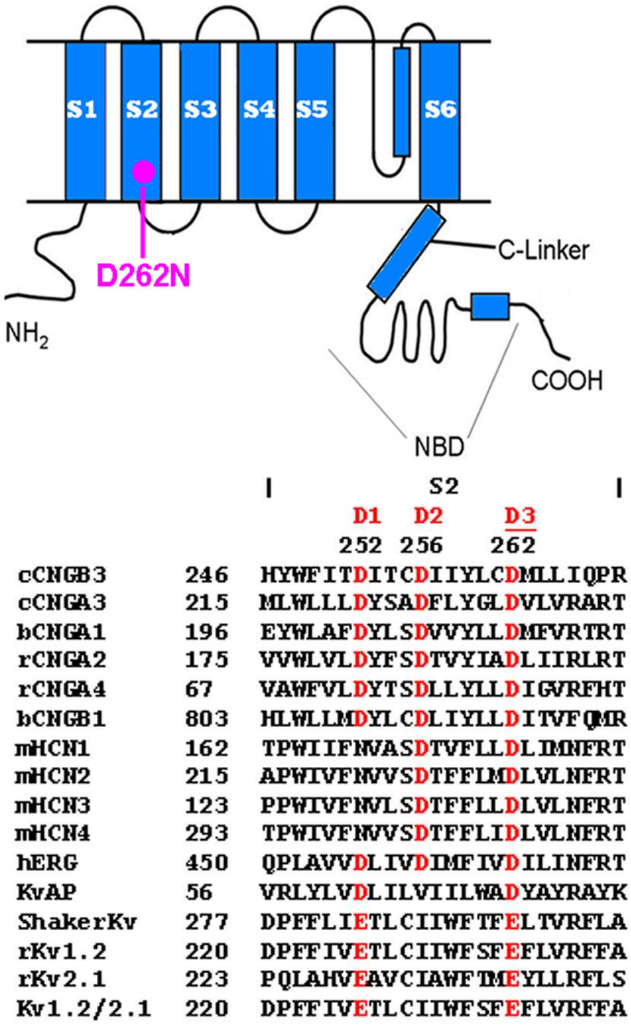

Figure 3.1 Schematic of the canine CNGB3 subunit indicating the D262N mutation (top). The canine daylight blind missesne mutation resides in the S2 as indicated in pink. **Sequence alignment of the S2 domain of the canine B3 subunit residues defines the *Tri-Asp motif* (bottom).** Asp 252, 256 and 262 in canine B3 delineate the highly conserved Tri-Asp motif which is conserved in all CNG channels with relative positions 2 and 3 conserved in the HCN channels. The flanking positions 1 and 3 are acidic residues in the Kv channels aligned here. c = canine; b = bovine; h = human, r = rat; m = mouse. CNGA1 and CNGB1 are rod channels; CNGA2 and CNGA4 are channel subunits expressed in olfactory cilia.

3.2 Materials and methods

3.2.1 Mutagenesis

1) Primer design

The *cA3* and *hA3* gene are available in the eukaryotic expression vector, pEYFP-N1 (*cA3-Y* and *hA3-Y* respectively) and *hB3* is available in pcDNA3.1, also a eukaryotic expression vector but without a fluorescent tag (see CHAPTER 2). Using these template genes, primers were designed using NetPrimer (http://www.premierbiosoft.com) to generate point mutations as in Table 3.1. These primers were obtained from Eurofins mwg/operon.

Table 3.1 Primers to generate *Tri-Asp* mutant channels. Each of the *Tri-Asp* residues was substituted by a non-polar, polar, or charged amino acid at a time. Res = residue, Mut = mutant, -r = reverse, c = canine, h = human.

Res	Mut	Gene	Primer	Primer sequence (5' – 3')
D1	C	*hA3-Y*	hA3-D207C	GGCTGGTCCTGTGCTACTCGGCAGATGTCC
			hA3-D207C-r	GGACATCTGCCGAGTAGCACAGGACCAGCC
	E	*hA3-Y*	hA3-D207E	GACATCTGCCGAGTATTCCAGGACCAGC
			hA3-D207E-r	GACATCTGCCGAGTATTCCAGGACCAGC
D2	I	*cA3-Y*	cA3-D225I	CCTGGACTACTCGGCAATTTTCCTCTATGGCTTGG
			cA3-D225I-r	CCAAGCCATAGAGGAAAATTGCCGAGTAGTCCAGG
	N	*cA3-Y*	cA3-D225N	CCTGGACTACTCGGCAAATTTCCTCTATGGCTTGG
			cA3-D225N-r	CCAAGCCATAGAGGAAATTTGCCGAGTAGTCCAGG
	C	*hA3-Y*	hA3-D211C	GACTACTCGGCGTGTGTCCTGTATGTCTTGG
			hA3-D211C-r	GGACATCTGCCGAGTAGCACAGGACCAGCC
	E	*cA3-Y*	cA3-D225E	CCTGGACTACTCGGCAGAGTTCCTCTATGGCTTGG
			cA3-D225E-r	CCAAGCCATAGAGGAACTCTGCCGAGTAGTCCAGG
D3	N	*hA3-Y*	cA3-D217N	GATGTCCTGTATGTCTTGAATGTGCTTGTACGAGC
			cA3-D217N-r	GCTCGTACAAGCACATTCAAGACATACAGGACATC
	N	*cA3-Y*	cA3-D231N	CCTCTATGGTTGAATGTGCTGGTGCGAGC
			cA3-D231N-r	GCTCGCACCAGCACATTCAACCATAGAGG
	N	*hB3*	hB3-D267N	CATCTACCTTTATAATATGCTATTTATCCAGCCC
			hB3-D267N-r	GGGCTGGATAAATAGCATATTATAAAGGTAGATG
	E	*hA3-Y*	hA3-D217E	CCTGTATGTCTTGGAGGTGCTTGTACGAGCTCGG
			hA3-D217E-r	CCGAGCTCGTACAAGCACCTCCAAGACATACAGG
	E	*cA3-Y*	cA3-D231E	CTATGGCTTGGAGGTGCTGGTGCG
			cA3-D231E-r	CGCACCAGCACCTCCAAGCCATAG

2) Polymerase Chain Reaction (PCR)

These mutant constructs were generated by PCR. Each PCR reaction contained 5 μl of 10x PFU buffer (Agilent), 50 ng of the template gene, 120 ng of the forward primer,

120 ng of the reverse primer, 1 µl of 10 mM dNTPs Mix (Invitrogen), and nuclease-free H_2O added to raise the total volume to 50 µl. For each cycle, the temperature was set to 95 °C for 30 seconds for DNA denaturation, to 58 °C for 1 minute for primer annealing, and to 68 °C for 14 minutes for primer extension. PCR was performed for 12 – 16 cycles.

3) Transformation using heat shock

Three µl of the PCR product as well as 2 µl of 0.3 M β-mercaptoethanol was added into 50 µl of *.E coli* cells, Library Efficiency® DH5α Competent Cells (Invitrogen) in an Eppendorf tube and kept on ice for 30 minutes. The tube was placed in 42 °C water bath for 45 seconds and was put back on ice for 2 minutes. The transformed cells were incubated in S.O.C medium (Invitrogen) for one hour in a shaker at 37 °C. The cells in S.O.C medium were plated on a LB agar plate (10g tryptone, 5g yeast extract, and 10g NaOH in 1L H_2O plus 15g agar) with 50ng/ml kanamycin and were grown over night. A colony was picked and grown in 5ml LB medium (10g tryptone, 5g yeast extract, and 10g NaOH in 1L H_2O) with kanamycin in a shaker at 37 °C for 5 - 7 hours, and of which 100 µl was inoculated and grown in 100 ml LB medium with antibiotic for selection overnight.

4) DNA purification

The gene in the vector was extracted using QIAGEN Plasmid Midi Kit (QIAGEN), and the full length gene was sequenced and confirmed using a set of

sequence primers designed as in Table 3.2. Sequencing was ordered to and performed by GENEWIZ.

Table 3.2 Sequencing primers for canine CNGA3, human CNGA3, and human CNGB3. A set of primers were designed to sequence the full length of each gene. The antisense sequencing prime reads the sequence on the antisense. c = canine, h = human.

Gene	Sequencing primer (SP)	Primer sequence (5' – 3')
cA3	cA3-SP-606 (antisense)	GCACACCAGCAGACACCAG
	cA3-SP1-397	AGAAACAACAACAACAACTG
	cA3-SP2-1154	CCCCTGTAAAAGATGAGGAGTACGTG
hA3	hA3-SP-619 (antisense)	CCAGGACCAGCCACAGCATCAGG
	hA3-SP1-375	GCCAGCAGACAGAGGGAGAAGCG
	hA3-SP2-1104	GACCCCACCCCCCGTGAAAG
	hA3-SP3-1583	CCGTGGTGGCTGATGATGGGGTC
hB3	hB3-SP-828 (antisense)	CTGGAGTCTGGGCTGGATAAATAG
	hB3-SP1-662	GGCTCTTGCTTGTCACTCTTGC
	hB3-SP2-1514	CGGTCCAGTTAGCCCTCGCC

3.2.2 Heterologous Expression

CNG channels were expressed heterologously as described in Chapter 2.2.2. tSA201 cells were raised and grown on coverslips in the culture medium. The cells were transfected with 1 - 2 µg of each *cA3-Y* (or *hA3-Y*) mutant gene or co-transfected with 1 - 2 µg of the wild-type *cA3-Y* gene and 2 - 4 µg the *hB3-D3/N* mutant gene employing Lipofectamine™ 2000 (Invitrogen). After transfection, the cells were grown at 37 °C for 24 – 48 hours.

3.2.3 Electrophysiology

cAMP and cGMP activated currents were measured and analyzed as described in Chapter 2.2.3. Inside-out patches were performed on transfected cells using glass electrodes with resistances of 1.2 - 4.2 MΩ, in a bath and electrode solution containing 120 mM NaCl, 2 mM EDTA, 2 mM EGTA, and 5 mM Hepes at pH 7.4. Saturating concentrations of cGMP and cAMP, 20 µM and 5000 µM respectively, were added to the bath. A series of 300-ms voltage pulses in 10-mV steps between - 100 mV and 100 mV. Currents were recorded at room temperature with an amplifier (AXOPATCH 10) and digitizer (DIGIDATA 1322A) and were analyzed on computer software (Clampfit 10.0™, Table curve™, Sigmaplot™).

3.2.4 Immunocytochemistry

Localization studies were performed as previously described (Patel et al., 2005). Approximately, 24 hours after transfection, cells on coverslips were immerged in PBS for 5 minutes and washed with PBS 2 more times and fixed with 4% paraformaldehyde in PBS for 20 minutes. After washed with PBS 3 times, the coverslips were mounted on slides using Vectashield® (Vector Laboratories, Inc.). Fluorescent cells were counted under 40x and photographed at 100x in a fluorescent microscope (Nikon). Unpaired t-tests were performed by QuickCalcs (http://www.graphpad.com).

3.3 Results

3.3.1 Electrophysiological properties of canine CNGA3-D3/N and canine CNGA3 + human CNGB3-D3/N

Loss of channel function was apparent in patches from cA3-D3/N homomeric channels in which no cGMP-activated currents were seen as in Figure 3.2. When cA3 was co-expressed with hB3-D3/N (a mutation generated using the residue 267 in human B3, the equivalent to residue 262 in *cB3*), the results were unexpected. In ~ 60% of the patches monitored, nucleotide-activated currents were recorded. However, these patches matched the characteristics of homomeric channels. Our working hypothesis is that when cA3 is co-expressed with hB3-D3/N, ~ 40% of the channels are heteromeric and do not express cGMP-activated currents. The remaining channels are homomeric cA3 channels, matching the characteristics reported in Table 3.3.

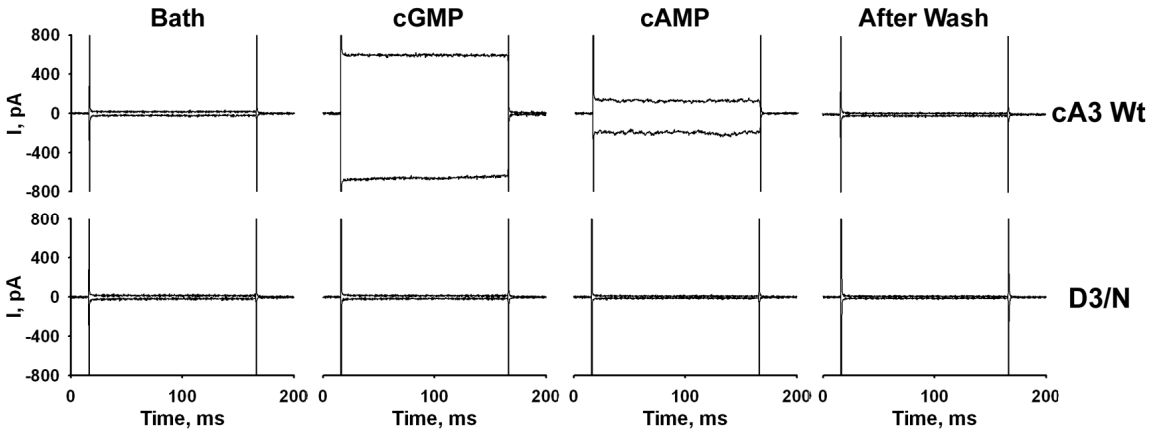

Figure 3.2 Cyclic nucleotide-activated currents in canine CNGA3 and canine CNGA3-D3/N mutant channels. Excised patch clamping showed no activated currents in the mutant channels at - 60 and + 60 mV. Currents were recorded in the presence of saturating concentrations of cGMP and cAMP, 200 μM and 5000 μM respectively, at - 60 mV and 60 mV.

Table 3.3 Nucleotide-activation of channels comparing wild-type and mutant subunits. The cAMP efficacy of patches from co-transfected (cA3 + hB3-D3/N) cells is consistent with these cells expressing homomeric cA3 channels. c = canine, h = human.

	cA3	cA3 + hB3	cA3-D3/N	cA3 + hB3-D3/N
cGMP Responses	**100% (33)**	**100% (25)**	**0% (15)**	**60% (10)**
cAMP Responses	**100% (33)**	**100% (25)**	**0% (14)**	**60% (10)**
I_{cA}/I_{cG}	**0.19 ± 0.01 (33)**	**0.33 ± 0.02 (25)**	**N/A**	**0.15 ± 0.01 (4)**

3.3.2 Cellular localization of canine CNGA3-D3/N and canine CNGA3 + human CNGB3-D3/N

The loss of function of canine A3-D3/N channels might be due to improper synthesis and folding, channel assembly and/or trafficking. The presence of a fluorescent tag on the cA3 subunit provided a way to investigate cellular localization of the CNG channels. Figure 3.3 shows the expression of YFP-tagged cA3 subunits in individual cells; averaged data are shown in the histograms (Figure 3.4). The large Golgi-like organelles and the membrane fluorescence are typical of canine A3 channels expressed alone or with human B3. Few intracellular aggregates are apparent in cells expressing wild-type subunits; however, the histogram data show a small but significant increase in the fraction of cells expressing intracellular aggregates when hB3 is co-expressed with canine A3.

The phenotype of the canine A3-D3/N homomeric channels is clear: very few cells express membrane or Golgi fluorescence and nearly 100% express intracellular aggregates (Figure 3.3). The expression pattern of cA3 with the hB3-D3/N is different

from the canine A3-D3/N mutation. As argued previously, a significant fraction of cells transfected with cA3 + hB3-D3/N show currents that match those from homomeric cA3 channels. It seems likely that the reduction in the fraction of cells expressing intracellular aggregates reflects cells that are expressing cA3 alone. The micrograph supports this possibility with one of the two cells shown in the right panel expressing Golgi with no intracellular aggregates; the other cell expresses only aggregates.

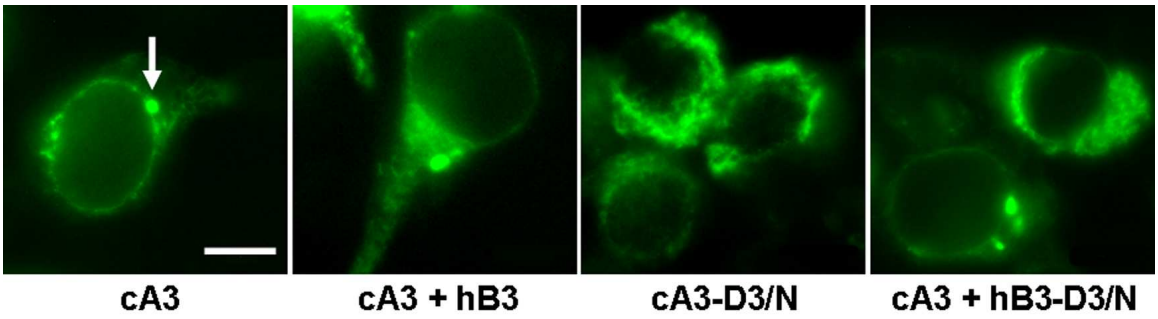

Figure 3.3 Cellular localization of YFP-tagged canine CNGA3constructs: canine CNGA3, canine CNGA3-D3/N, canine CNGA3+ human CNGB3, and canine CNGA3 + human CNGB3-D3/N. Clear, significant differences are seen with expression of mutant D3/N subunits although see text for the interpretation of the cA3 with hB3-D3/N mutant subunit. The arrow indicates a Golgi-like organelle, and the scale bar is 10 μm.

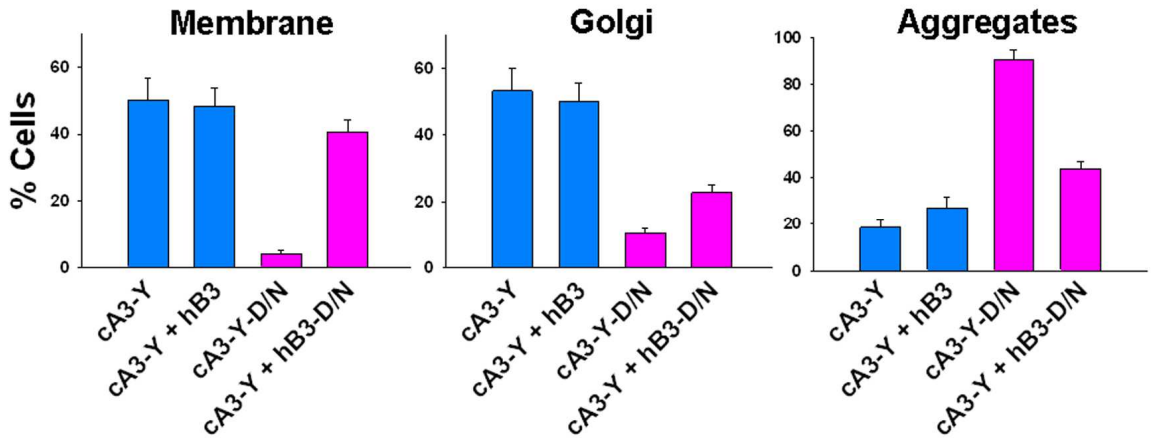

Figure 3.4 Averaged expression characteristics are shown in histograms. Histograms were constructed from counts of >800 cells. The cA3 and cA3 + hB3 expression patterns have a small but significant increase in intracellular aggregates ($p = 0.02$ on unpaired t-test). Mutant D3/N subunits increase the number of intracellular aggregates. Wild-type channels = blue, mutant channels = pink.

3.3.3 Electrophysiological properties and Cellular localization of CNGA3 *Tri-Asp* mutant channels

Mutant canine and human A3 subunits were generated by substituting each of the three D residues with a non-polar isoleucine (I), an uncharged polar amino acid cysteine (C) or asparagine (N), and an acidic glutamic acid (E) as in Table 3.4. Patch clamp analysis showed that none of the mutant A3 channels expressed cGMP-activated currents. Most surprising, glutamic acid substitutions at D1, D2, or D3 positions produced no functional channels despite conserving the negative charge of the side chain. Localization studies showed a dominance of intracellular aggregates in all the mutant channels, indicating mislocalization (Table 3.4 and Figure 3.5).

Table 3.4 Summary of electrophysiology and localization studies on *Tri-Asp* mutant channels. Results support an altered fluorescence localization with at least 200 cells counted for each mutant. + = normal (wild-type) phenotypes; currents for cGMP and cAMP, and Golgi and membrane fluorescence for localization. – = abnormal (mutant) phenotypes; no currents for cGMP and cAMP, and intracellular aggregates for localization.

Residue	Mutation	cGMP	cAMP	Localization
Wt		+	+	+
D1	C	–	–	–
	E	–	–	–
D2	I	–	–	–
	C	–	–	–
	N	–	–	–
	E	–	–	–
D3	N	–	–	–
	E	–	–	–

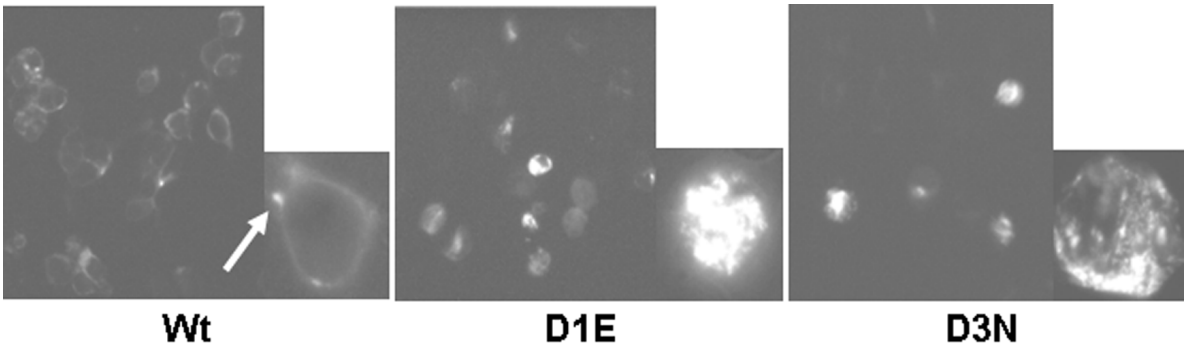

Figure 3.5 Cellular localization of human CNGA3 and Asp mutants. Wild-type hA3 localized to membrane and Golgi whereas all mutants showed cytoplasmic aggregation. Membrane fluorescence was absent in nearly all fields for the Asp mutants consistent with improper trafficking. The arrow indicates a Golgi-like organelle.

3.4 Summary

3.4.1 Loss of channel function and mislocalization in all the *Tri-Asp* mutant channels

The canine missense mutant as well as all the Asp mutant channels in the *Tri-Asp motif* resulted in loss of channel function and mislocalization in heterologous expression. The results of these *Tri-Asp* mutations can be compared with a previous study in which achromatopsia mutations in the S1 resulted in loss of function and retention of the mutant hA3 subunits in the ER (Patel et al., 2005). Other CNG channel mutations recognized in patients with achromatopsia show similar loss or alterations of channel function associated with defects in folding, cellular localization and/or trafficking (Ding et al., 2010; Matveev et al., 2010; Patel et al., 2005; Saliba et al., 2002). Mislocalization and misfunction are considered to be typical phenotypes of channelopathies in general (Ashcroft, 2006). The results from heteromeric mutant channels, cA3 + hB3/N, also showed an increase in intracellular aggregates, yet need an explanation.

3.4.1 Difference in the functional role of acidic residues of the *Tri-Asp motif* in CNG and voltage-gated K^+ channels

The results of the *Tri-Asp* mutations can be further considered and analyzed in light of results from related voltage-gated K^+ channels. Neutralizing even a single Asp residue in S2 caused the channel to be completely dysfunctional, and any of the Glu substitutions also produced no functional channels despite conserving the negative charge. These complete negative results are inconsistent with a voltage-gated Shaker K^+

channel study. In that study, the function was altered but not eliminated when Glu at positions D1 and D3 were substituted by Asp (Sang-Ah Seoh, 1996). Similarly, in Shaker and human Ether-a-go-go-Related Gene channel (hERG), a neutralizing alteration in position D1 or D3 alters but does not eliminate channel function (Pless et al., 2011; Seoh et al., 1996; Zhang et al., 2005). Thus, I observe a difference in the functional role of the Asp residues in CNG channel *Tri-Asp motif* and voltage-gated K^+ (Kv) channels. In conclusion, the S2 *Tri-Asp motif* in CNG channels appears critical for folding and assembly as well as trafficking and function. Future studies may shed more light on the role of this motif in subunit biogenesis and remain to be resolved.

CHAPTER 4

HOMOLOGY MODEL OF CANINE CNGA3 CHANNEL WITH MOLECULAR DYNAMICS SIMULATIONS

4.1 Introduction

4.1.1 Insights on channel structure and function gained from crystal strictures and computational science

In 1998, Roderick MacKinnon and colleagues performed X-ray crystallography and, for the first time, determined the three-dimensional structure of a K^+ channel from bacteria, *Streptomyces lividans* K^+ channel, Kcsa (Doyle et al., 1998). Since the initial channel structure, more X-ray crystal structures of channels, such as *Aeropyrum Pernix* K^+ channel, KvAP (Lee et al., 2005) and bacterial cyclic nucleotide-regurated channel, MlotiK1 (Clayton et al., 2008), have been determined, providing a great deal of insight into channel structure. Furthermore, these structures have been relaxed and studied in a virtual lipid membrane using molecular dynamics (MD) simulations to predict what the channel structure and function would be like in a native environment. Although MD simulations do not reflect exactly what happens in physiology, it is a very good way to hypothesize potential conformational changes or interactions between molecules which often can be tested experimentally.

Despite my efforts to investigate the role of the *Tri-Asp motif*, all the *Tri-Asp* mutations resulted in the loss of channel function and mislocalization. Being experimentally dead-locked led me to think of exploring computational approaches.

However, no high-resolution structure of the transmembrane region of any eukaryotic CNG channel is available to date. As an alternative, to gain a first insight into the role of the *Tri-Asp motif*, and in particular of D3 in CNG channels, I decided to first create a homology model of a cone CNG channel and relax it with MD simulations.

4.1.2 Creating a homology model of canine CNGA3 homomeric channel

I chose to build a homology model of the cA3 homomeric channel because cA3 is able to form functional homotetramers and was as shown by our electrophysiology and immunocytochemistry experiments. It therefore provides a simplified model of cone CNG channels. We later propose to extrapolate the bulk of the results to other mammalian CNG subunits, and cB3 more specifically.

To determine a template structure for a cA3 homology model, PSI-Blast search was performed over the Protein Data Bank Database (Altschul et al., 1990). As a result, the chimeric voltage-gated potassium channel, Kv1.2/2.1 (2R9R), was identified as the closest match for a protein of a known structure (Long et al., 2007). Therefore, the Kv1.2/2.1 high resolution crystal structure was used as a template structure. A standard MODELLER (Eswar et al., 2006) routine was then used to create a homology model of the transmembrane region of the cA3 channel, comprising the four auxiliary domains (S1 – S4, corresponding to the voltage-sensing domains in Kv1.2/2.1) and the pore domain (S5 – S6).

4.1.3 Relaxing the model with molecular dynamics (MD) simulations

The MODDELER (Eswar et al., 2006) creates a homology model using the X-ray crustal structure of a template and the amino acid sequence alignment of the protein of interest with the template protein. Thus, the homology model will turn out to be exactly like the template structure, except the side chains and their angles are free to move. The amino acid sequence of the protein of interest is, however, not the same as that of the template, and hence the interactions between residues should be different. Moreover, the channel protein physiologically resides in the transmembrane with water molecules and ions on both intra- and extracellular sides which should be taken into account for interactions with the protein residues as well. To predict how the channel behaves in its physiological environment, molecular dynamics (MD) simulations were employed. MD simulation provides us a great means to predict protein structure and function by applying dynamics using equations for the motion of an individual atom (Lindahl, 2008).

First, we placed the homology model in a membrane patch, palmitoyl-oleyl-phosphatidylcholine (POPC), which is the most commonly used membrane type for channel protein simulations. 120 mM Na^+ and Cl^- as well as water molecules were then added on both intra- and extracellular sides to mimic our experimental conditions.

The small size of the simulated system necessarily raises problems concerning potential boundary effects. To avoid these problems, it is customary to apply periodic boundary conditions (PBC). Under these conditions, the box of the simulation system is replicated and added to the system endlessly along the x, y, and z axes so that there

would be no vacuum effects. Molecules on one edge of the box behave as if one edge is seamlessly connected to the edge on the opposite side.

MD simulations were performed in the isothermal-isobaric ensemble that conserves moles (N), pressure (P), and temperature (T) (Parrinello and Rahman, 1980; Lindahl, 2008). This NPT ensemble requires a thermostat and a barostat to mimic experimental conditions with the ambient temperature of 298K and the pressure of 1 atm. Interactions of particles in the simulation are referred to as force fields. The simulation used the CHARMM22-CMAP force field with torsional cross-terms for the protein (MacKerell et al., 1998) and CHARMM27 for the phospholipids (MacKerell et al., 2004).

4.2 Materials and methods

4.2.1 Amino acid S1 – S6 sequence alignments of canine and human CNGA3 and CNGB3 with Kv1.2/2.1

Amino acid sequences of canine A3 (GI: 345777245), human A3 (GI: 4502917), canine B3 (GI: 50978664), and human B3 subunit (GI: 116642889) were aligned with the secondary structure of the Kv1.2/2.1 (GI: 16087792) using Clustal X version 2.0.1. (Larkin et al., 2007) (http://www.clustal.org/). The blocks of amino acid substitution matrix was used, together with standard parameters (opening gap penalty of 10, gap extension penalty of 0.20, and gap distance of 5). The S1 – S6 transmembrane domains were then assigned according to the crystal structure of Kv1.2/2.1 (2R9R).

4.2.2 Homology Modeling

The procedure described here was previously used to build a model of the transmembrane segments of Nav1.4 (Gosselin-Badaroudine et al., 2012). Briefly, the best template available to model the transmembrane domains of canine A3 was identified by a PSI-BLAST search over the Protein Data Bank Database (Altschul et al., 1990). Among the hits, the Kv1.2/2.1 high-resolution structure released in 2007 (Long et al., 2007) was the candidate bearing the transmembrane domains with the highest max score. A standard MODELLER (Eswar et al., 2006) routine was then used to build a comparative model of the transmembrane region of the cA3 channels. Because the channel is a homotetramer, we enforced tetrameric symmetry between the Cα atoms of the four subunits. To direct the charged residues of the auxiliary domains away from the

lipid/protein interface and have them point toward the hydrated lumen, we enforced distance restraints between pairs of postitively/negatively charged residues in cA3: (K259(S3)/D221(S2), K294(S4)/D221(S3), K259(S3)/D225(S2), R297(S4)/D225(S2), R252(S3)/D231(S2), R235(S2)/D249(S3), K248(S3)/D303(S4), K255(S3)/E300(S4). These pairs were chosen after an initial unrestrained model was equilibrated with MD simulations (see below) enabling us to identify most probable contacting pairs while excluding those that would cause unfavorable conformations. D398 located at the extracellular end of S6 was directed upwards, towards S373 (pore loop) in order to avoid water protrusion in the membrane region. The pair of contacting residues E306 (S4 – S5 linker) and R424 (S6) was pulled together by enforcing distance restraints. The Pro residue that defines the break in the S3 helix of Kv1.2/2.1 is absent in the CNG channels, which likely indicates that S3 is entirely helical (no break between S3a and S3b as in the template). We therefore enforced helicity of the S3 segment.

4.2.3 Molecular Dynamics (MD) Simulations

The homotetromeric cA3 channel was inserted in a fully hydrated palmitoyl-oleoyl-phosphatidyl-choline (POPC) bilayer (280 lipid molecules, 31294 water molecules, 79 Cl^- ions, 71 Na^+ ions, and the total size of the system is 147992). The systems were equilibrated under normal constant temperature and pressure conditions (298 K, 1atm) in a 120 mM NaCl solution using the following scheme: The lipid tails were first melted while keeping the rest of the atoms of the system fixed during 300 ps. Then, to ensure correct reorganization of the lipids and solution, the positions of all of the

atoms of the channel were constrained during 0.5 ns. In a third step, the side chains were allowed to reorganize while the backbone was kept restrained (5 ns with a 1 kcal/mol/Å^2, 5 ns with a 0.5 kcal/mol/Å^2 force constant and 5 ns with a 0.1 kcal/mol/Å^2 force constant). During this time, hydration of the membrane-protein interface was prevented. For cA3, this step is crucial, due to the high number of charged residues in transmembrane position. Next, the channel was relaxed while keeping a harmonic constraint on the backbone of the S4 helix for 65 ns. Finally, a 65-ns unrestrained MD simulation of the entire channel was conducted, enabling full relaxation of the system. The MD simulations were carried out using the program NAMD2.9 (Phillips et al., 2005). Langevin dynamics was applied to keep the temperature (300 K) fixed. The equations of motion were integrated using a multiple time-step algorithm (Izaguirre et al., 1999). Short- and long-range forces were calculated every 1 and 2 time-steps respectively, with a time step of 2.0 fs. Chemical bonds between hydrogen and heavy atoms were constrained to their equilibrium value. Long-range electrostatic forces were taken into account using the particle mesh Ewald approach (Darden et al., 1993). The water molecules were described using the TIP3P model (Jorgensen et al., 1983). The simulation used the CHARMM22-CMAP force field with torsional cross-terms for the protein (MacKerell et al., 1998) and CHARMM27 for the phospholipids (MacKerell et al., 2004). The simulations were performed on Owlsnest, Temple University's supercomputing facilities.

4.3 Results

4.3.1 CNG channel amino acid sequence alignment and predicted transmembrane topology of canine CNGA3 and CNGB3

The S1 – S6 transmembrane regions of the cone CNG channel subunits were aligned as described above; the alignment for the human and canine subunits is shown in Figure 4.1. As expected, the pore regions share a high degree of similarity. The signature sequence of the K^+ selectivity filter (TVGYG) is lost in CNG channels, accounting for their relatively low ion selectivity. One striking difference between the cA3 and the template Kv1.2/2.1 is the larger number of charged residues located in the transmembrane segments of S2 – S4. S1, on the other hand, only contains two positively charged residues at each extremity, which are anticipated to be involved in anchoring to the membrane headgroups. Also, the proline residue that defines the break between the two helices S3a and S3b of Kv1.2/2.1 is absent in cA3 channels, suggesting that S3 may be a continuous helix.

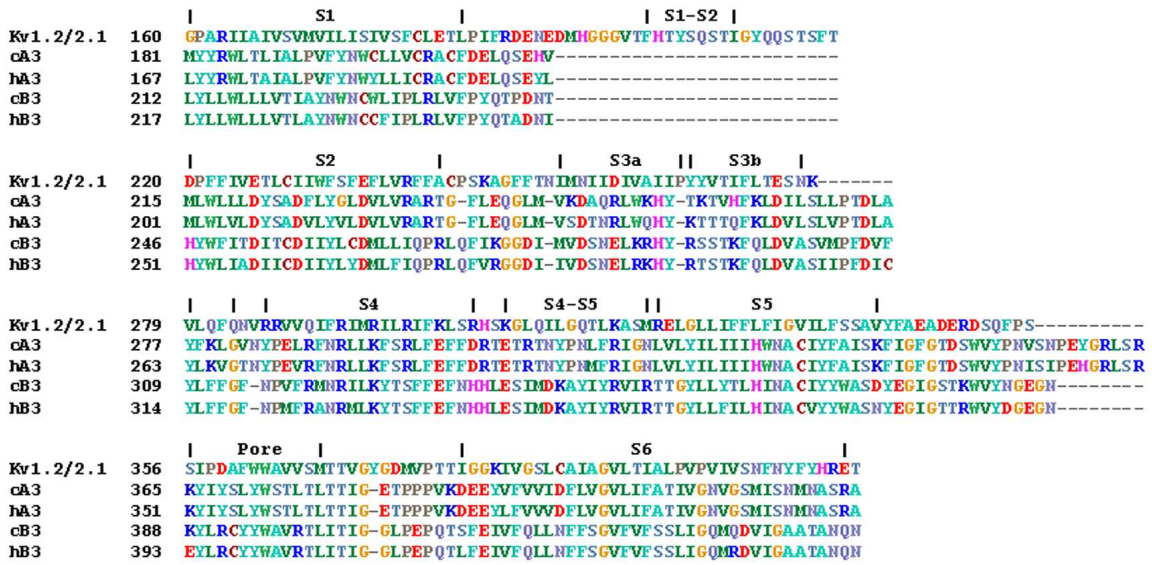

Figure 4.1 Predicted topology of the transmembrane regions of canine and human CNGA3 and CNGB3 subunits. The transmembrane domains are defined by the crystal structure of the chimeric voltage-gated potassium channel Kv1.2/2.1 (2R9R). The amino acid sequence identity between the cA3 and hA3 is 82% and is 76% between cB3 and hB3. c = canine, h = human.

4.3.2 Homology model of canine CNGA3 channel relaxed with molecular dynamics simulations

1) Homology modeling of canine CNG channel

One main difference between cA3 and Kv1.2/2.1 is the large number of charged residues located in S2 – S4 (12 positive and 9 negative charges), compared to 8 positive and 5 negative charges in Kv1.2/2.1. In Shaker channels, crystal structures have shown that these charged residues are shielded away from the unfavorable lipid environment and are rather involved in salt bridge pairings and pointing towards the center of the solvated 4-helical bundle. Accordingly, to build the homology model, we enforced distance restraints between pairs of positively and negatively charged residues (see Materials and

methids for details). Similarly, because the proline residue that defines the break in the S3 helix of Kv1.2/2.1 is absent in canine A3 channels, we enforced helicity of the S3 segment. This results in directing the charges of S2 – S4 towards the hydrated lumen of the four helix bundle. These constraints were initially imposed during the equilibration phase of the MD simulations and gradually released (see Materials and methids for details).

2) Overview of the canine CNG channel model relaxed by molecular dynamics simulations

The canine A3 channel shares a similar topology with the Kv1.2/2.1 template, with the tetrameric assembly of S5 – S6 defining the pore and S1 – S4 defining four auxiliary domains (Figure 4.2 (A)) distributed around the pore assembly. The central axis of the pore defines the non-selective conduction pathway for cations. Figure 4.2 (B) shows the arrangement of the lipid bilayer membrane around the tetrameric channel and play a role in stabilizing the tertiary and quaternary fold. Figure 4.3 also shows the arrangement of the lipid bilayer membrane around the tetrameric channel from the side.

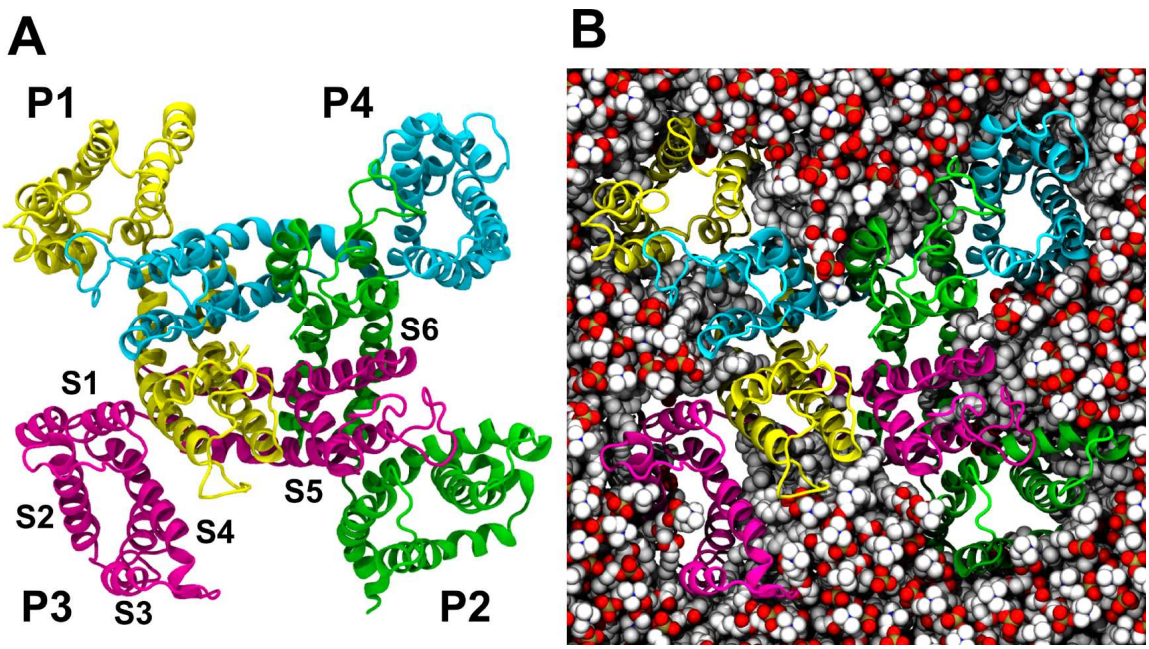

Figure 4.2 Structural model of the canine CNGA3 homotetramer in its environment.
(A) Top view: The four subunits are represented as ribbons. P1 is colored in yellow, P2 in green, P3 in pink and P4 in cyan. Side chains are omitted for clarity. The tetrameric assembly of the two N-terminal helices S5 and S6 forms the central pore. The other transmembrane segments (S1-S4) of each subunit forms a bundle located at the periphery of the pore.
(B) Top view: The protein is represented as in (A). The POPC lipids embedding the channel are represented as VDW spheres, with carbons in white, phosphates in brown, oxygens in red and nitrogens in blue. Water molecules and ions are not shown for clarity.

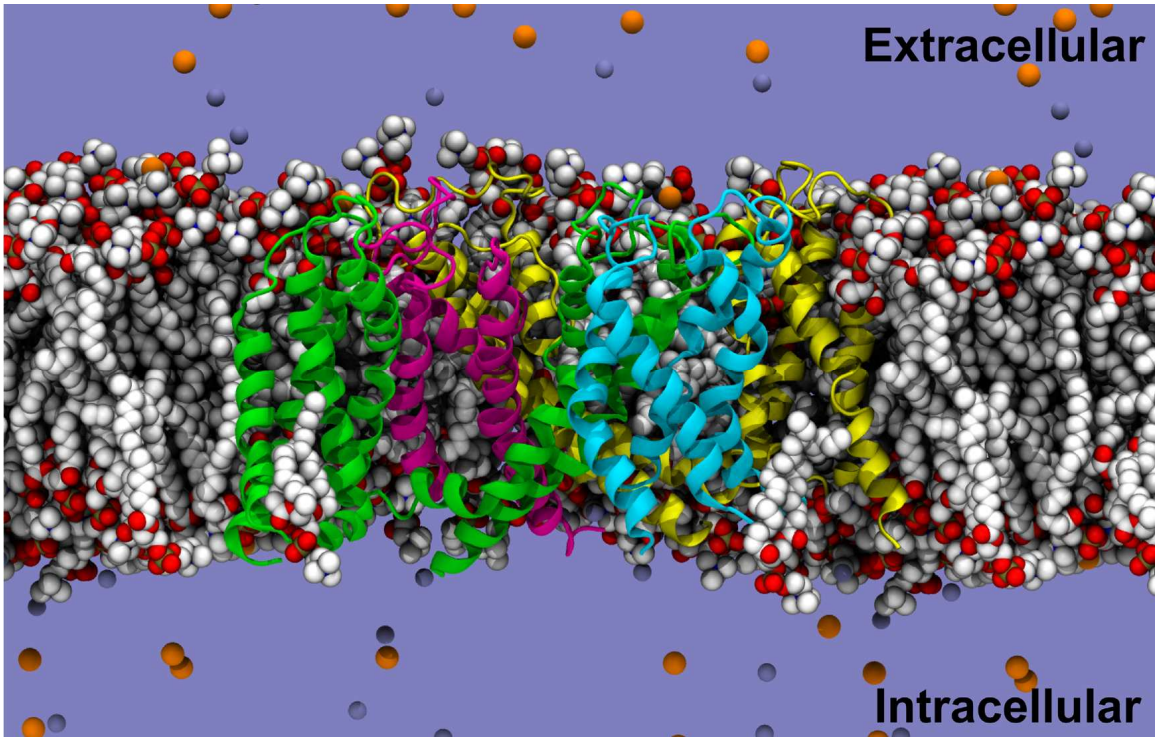

Figure 4.3 Side view of canine CNGA3 model in its environment: The protein and the lipids are represented as in Figure 4.2 (A). The contours of the water-filled volume are represented as a transparent surface. The Na^+ ions are in orange and the Cl^- in purple. The extracellular domain is located at the top and in the intracellular domain is located at the bottom.

3) *Tri-Asp motif* in S2 and charged residues of the S1 – S4 bundle

As can be inferred from Figure 4.4, the *Tri-Asp motif* is located on the S2 segment of the vestigial voltage-sensing domain and D3 is the intracellular-most charge. The rest of S2, S3 and S4 also contain a large number of charges of both signs. Figure 4.5A reveals that all the charges point toward the center of the voltage-sensing domain. As in Shaker channels, these charges are stabilized in transmembrane position through salt bridge pairings. Such a pairing mechanism is thought not only to be important for function but also for proper folding.

Also, it is apparent that the charges are organized in two separate clusters: the extracellular cluster contains D266, E286, D221 (D1) and D225 (D2) as negative charges and R288, K264, R291, K259, K294 and R297 as positive charges; the intracellular cluster contains D231 (D3), E300, E303 and D249, and K255, R252, R304, K248, R235 and R237. Interestingly, the topology of the solvent accessible volume is shaped as an hourglass, with water protruding from the extracellular medium and from the intracellular one. The two clusters of charges are then solvated by the extra- and the intra-cellular half, respectively. Compared to Shaker channels in which the salt bridge network is well defined, here, due to the larger number of charges, however, many more salt bridge pairings can occur.

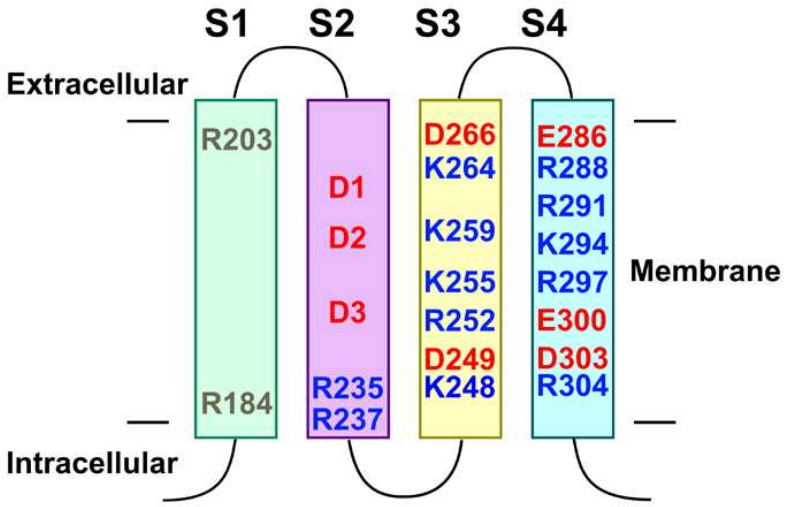

Figure 4.4 Topology of the S1 – S4 domain of canine CNGA3 subunit and localization of the charged residues. S1 is represented in green, S2 in purple, S3 in yellow and S4 in cyan. Charges not involved in salt bridging are shown in grey, other positive K and R are shown in blue, negative D and E are shown in red. D1, D2 and D3 correspond to D221, D225, and D231 in cA3, respectively.

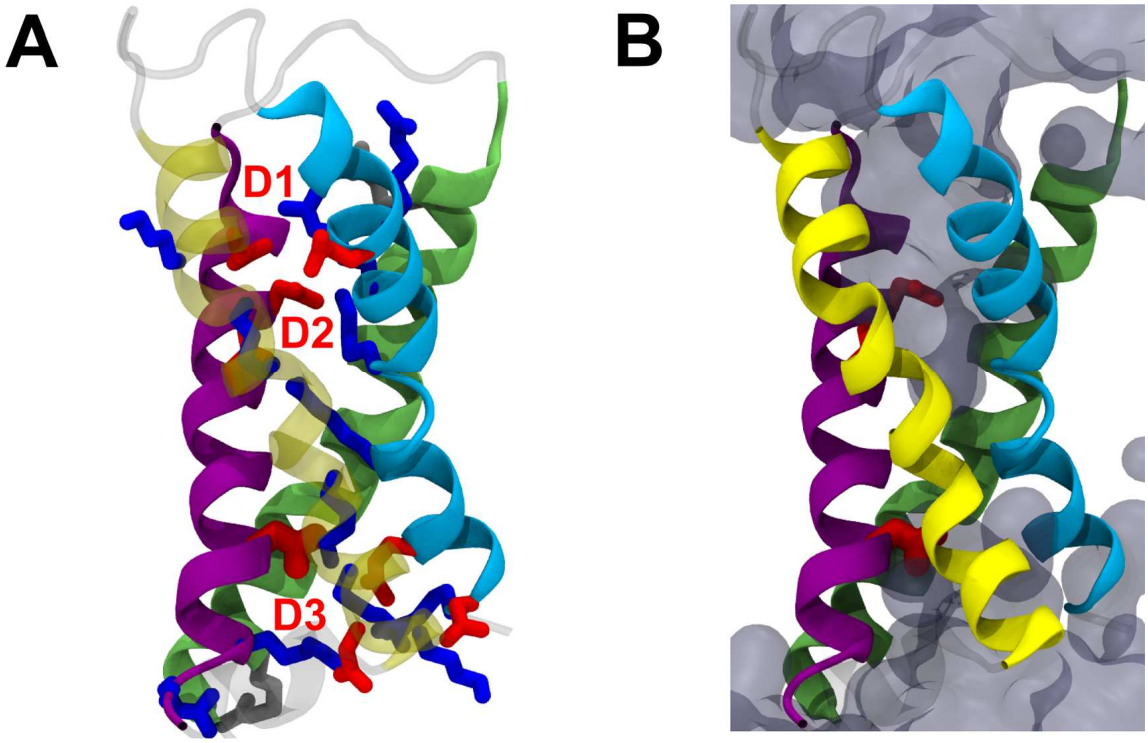

Figure 4.5 (A) Molecular model of a representative S1 – S4 domain with all charges of the bundle represented. Color coding is the same than in Figure 4.4. Positive charges are in blue, negative charges in red. The *Tri-Asp motif* residues are noted as D1, D2 and D3 in red. Note that this is a snapshot of the salt bridge network of the P4 subunit VSD. Lipids, water, and ions are omitted for clarity.
(B) Same as (A) with water. The *tri-Asp motif* residues are depicted as red rods, the solvent accessible volume is delineated by a transparent surface.

4) Global electrostatic equilibrium by unspecific slat bridge formation between the *Tri-Asp motif* and basic residues in S2 – S4

Figure 4.6 reports the distances between pairs of positive and negative charges during the last 20 ns of the equilibration. It demonstrates that, despite the fact that specific salt bridges were enforced during homology modeling and the initial steps of the equilibration, the S1 – S4 bundles in each of the subunits reached different

conformations. It can then be inferred from my model that each subunit has a unique pattern of salt bridge networks despite the 4-fold symmetry of the subunit organization. Further, the salt bridges in the cA3 model resemble a fixed lattice of pairings in contrast to the Shaker channel models that show salt bridge partners changing during the channel opening. Therefore, contrary to Shaker channels, it is not feasible to characterize the structure of the vestigial voltage-sensing domain by a single well-defined network of salt bridges.

Note that while the *Tri-Asp motif* is conserved in all other CNG subunits (Figure 3.1), and specifically in cB3, it is not the case for the charges in the other transmembrane segments. For example, the positive charge R235 in cA3 is lost in cB3 (I266); R252 in cA3 is reversed to a negative residue (E284) in cB3; R297 in cA3 is S328 in cB3 (Figure 4.1). While we do not expect the details of the cA3 structure to be conserved in cB3, because of the sequence similarity, we think that the coarse features of the structure of the vestigial VSD domain can be extrapolated to understand the effect of the D3/N mutation in cB3.

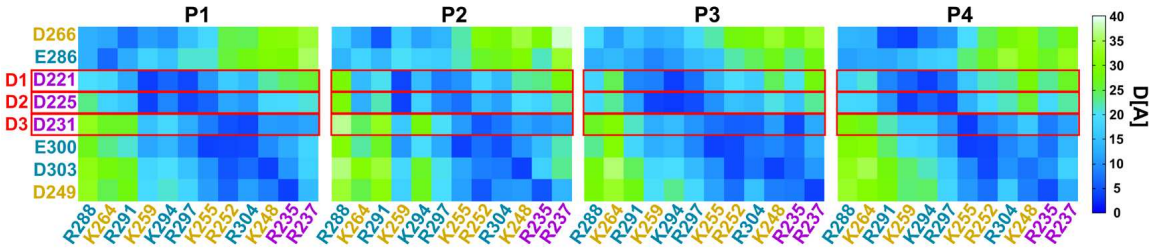

Figure 4.6 Mapping of the average distance between negative and positive residue pairs. The atom, NZ, is used for K, CZ for R, CG for D, and CD for E. Each subunit is presented separately. The distances were averaged over the last 20 ns of simulation. Distances range from 0 (deep blue) to 40 Å (light green). The charge labels are colored according to the transmembrane segment they belong to. Note that the salt bridge network is rather different from one subunit to the other, highlighting the presence of several conformational changes of similar stability.

4.4 Summary

4.4.1 Possible disruption of the global electrostatic equilibrium in the S1 – S4 bundle by any mutation in the *Tri-Asp motif*

Our experimental work suggests that the *Tri-Asp motif* in CNG channels is critical for folding, assembly, trafficking, and/or function. The homology model shows that the Asp residues of the *Tri-Asp motif* are involved in global electrostatic salt bridge networking formed by unspecific parings. If D3 (or D1 or D2) is mutated to an uncharged residue, we expect several salt bridges to be lost. Moreover, the imbalance between positive and negative charges will increase even more, leading to a probable destabilization of the entire domain. It may even be that the folded state of the protein becomes inaccessible.

In the folded canine A3 channel, our model reveals that the side chain interactions of the highly-conserved D3 are required for inter-helical contact through salt bridge pairing. D2 and D1 also make contact with the positive residues of S2 – S4, similarly to what is observed in Shaker channels. Therefore, considering the sequence and structural similarity between Shaker family members, we propose that mutation of D3 to an uncharged residue will likely also lead to protein misfolding.

CHAPTER 5

CANINE DAYLIGHT BLIND MISSENSE MUTATION, *CNGA3-R424W,* IN THE C-TERMINAL END OF S6

5.1 Introduction

5.1.1 Canine *CNGA3-R424W* misesense mutation in S6

Recently, Dr. Aguirre and colleagues identified another missense mutant, Arg (R) 262 to Trp (W), in the CNGA3 subunit of German Shorthair Pointer dogs associated with loss of cone ERG function and daylight vision. The equivalent mutation was previously identified in the hA3 gene, *hA3-R410W* (Wissinger et al., 2001). According to the amino acid sequence alignments of Shaker superfamily members (Figure 3.1 and Figure 5.1), the residue R424 is located in the C-terminal end of the S6. The Arg residue is conserved in CNGA1, A2, and A3 subunits as well as HCN channels. On the other hand, CNGA4 and Kv channels have the opposite negative charge, Glu (E). CNGB1 and B3 subunits as well as hERG have a polar residue, Gln (Q) and Thr (T) respectively.

Compared to the D262 N mutation in the cB3 subunit, this cA3-R424W mutation is more straight-forward to investigate because it is in the A-type subunit that can form functional homomeric channels. The effect of the mutation on channel properties was directly examined in cA3 subunit channels without heteromeric co-expression issues described in CHAPTER 3. In order to investigate the molecular properties of the missense mutation, we generated a *cA3-R424W*. We asked further whether substitution of the Arg 424 with Lysine (K), conserving the positive charge, could preserve channel

function and, similarly, whether the cA3 channel could tolerate substitution of the Arg 424 with the opposite negative charge, Glutamic acid (E) as in Kv channels. In addition, we predicted the structural and functional role of the Arg 424 residue using the homology model of the cA3 channel relaxed with MD simulations.

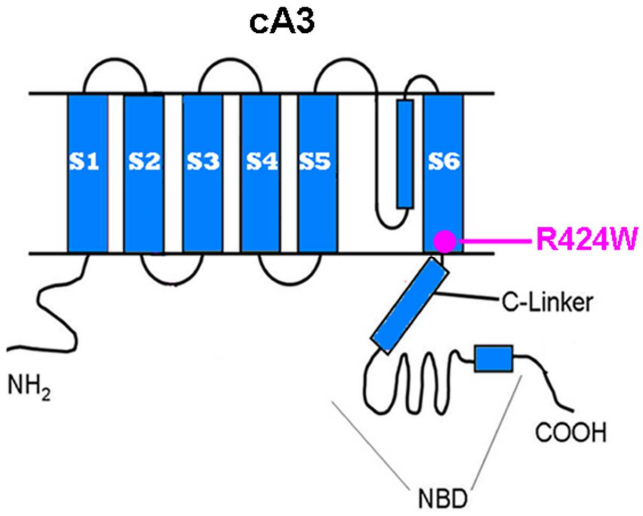

		S6			
				R	
				424	
cCNGA3	DEEYVFVVIDFLVGVLIFATIVGNVGSMISNMNASR				424
bCNGA1	DSEYFFVVADFLIGVLIFATIVGNIGSMISNMNAAR				405
rCNGA2	DEEYLFVIFDFLIGVLIFATIVGNVGSMISNMNATR				384
rCNGA4	EEEYLFMVGDFLLAVMGFATIMGSMSSVIYNMNTAD				276
bCNGB1	LFEIVFQGLNYFTGVFAFSVMIGQMRDVVGAATAGQ				1004
cCNGB3	SFEIVFQLLNFFSGVFVFSSLIGQMQDVIGAATANQ				447
mHCN1	MSDLWITMLSMIVGATCYAMFVGHATALIQSLDSSR				393
mHCN2	MTDIWLTMLSMIVGATCYAMFIGHATALIQSLDSSR				446
mHCN3	MPDVWLTMLSMIVGATCYAMFIGHATALIQSLDSSR				356
mHCN4	MSDVWLTMLSMIVGATCYAMFIGHATALIQSLDSSR				524
hERG	NSEKIFSICVMLIGSLMYASIFGNVSAIIQRLYSGT				670
KvAP	PIGKVIGIAVMLTGISALTLLIGTVSNMFQKILVGE				242
ShakerKv	VWGKIVGSLCAIAGVLTIALPVPVIVSNFNYFYHRE				488
rKv1.2	IGGKIVGSLCAIAGVLTIALPVPVIVSNFNYFYHRE				420
rKv2.1	LLGKIVGGLCCIAGVLVIALPIPIIVNNFS-EFYKE				418
Kv1.2/2.1	IGGKIVGSLCAIAGVLTIALPVPVIVSNFNYFYHRE				416

Figure 5.1 (Top) Schematic of the canine CNGA3 subunit indicating the R424W mutation. The canine daylight blind missesne mutation resides in the S6 as indicated in pink.

(Bottom) Amino acid sequence alignment of the S6 segment of Shaker superfamily channels defines the location of R424 in the canine CNGA3 subunit. cA3-R424 is the very last residue of S6. c = canine; b = bovine; h = human, r = rat; m = mouse. CNGA1 and CNGB1 are rod channels; CNGA2 and CNGA4 are channel subunits expressed in olfactory cilia.

5.2 Materials and methods

5.2.1 Mutagenesis

1) Primer design

The *cA3* gene is available in the eukaryotic expression vector (*cA3-Y*) as described in Chapter 2. Using this template gene, primers were designed using NetPrimer (http://www.premierbiosoft.com) to make point mutations as in Table 3.1. These primers were ordered from Eurofins mwg/operon.

Table 5.1 Primers to make canine CNGA3 Arg 424 mutant subunits. Arg 424 in the cA3 subunit was substituted by a non-polar, polar, or charged amino acid at a time. -r = reverse, c = canine.

Gene	Mutation	Primer name	Primer sequence (5' – 3')
cA3-Y	R424W	cA3-R424W	CGAACATGAATGCTTCATGGGCCGAGTTCCAGGCC
		cA3-R424W-r	GGCCTGGAACTCGGCCCATGAAGCATTCATGTTCG
	R424K	cA3-R424K	CGAACATGAATGCTTCAAAGGCCGAGTTCCAGGCC
		cA3-R424K-r	GGCCTGGAACTCGGCCTTTGAAGCATTCATGTTCG
	R424E	cA3-R424E	CGAACATGAATGCTTCAGAGGCCGAGTTCCAGGCC
		cA3-R424E-r	GGCCTGGAACTCGGCCTCTGAAGCATTCATGTTCG
	E306R	cA3-E306R	CTTTGACCGCACGAGGACGAGAACCAACTACCCC
		cA3-E306R-r	GGGGTAGTTGGTTCTCGTCCTCGTGCGGTCAAAG

2) Polymerase Chain Reaction (PCR)

These mutant channels were generated by PCR as described as CAPTER 3.2.1.

3) Transformation using heat shock

Transformation was performed as described as CAPTER 3.2.1.

4) DNA purification

DNA was extracted form E. coli cells as described as CAPTER 3.2.1.

5.2.2 Heterologous Expression

CNG channels were expressed heterologously as described in CAPTER 3.2.2.

5.2.3 Electrophysiology

cAMP and cGMP activated currents were measured and analyzed as described in CHAPTER 3.2.3.

5.2.4 Immunocytochemistry

Localization studies were performed as described in CHAPTER 3.2.4.

5.3 Results

5.3.1 Electrophysiological properties of canine CNGA3-R424W mutant channels

cA3-R424W homomeric mutant channels expressed no cGMP- nor cAMP-activated currents as in Figure 5.2 and Table 5.2. These results are expected for an achromatopsia mutation (refer to CHAPTER 3.4). An R424E mutation also led to loss of channel function. When the positive charge was conserved, however, 25 % of the cA3-R424K patches were responsive. These results are different than those of the *Tri-Asp* D3 mutations in which the conservation of the negative charge did not preserve channel function (refer to Summary for details).

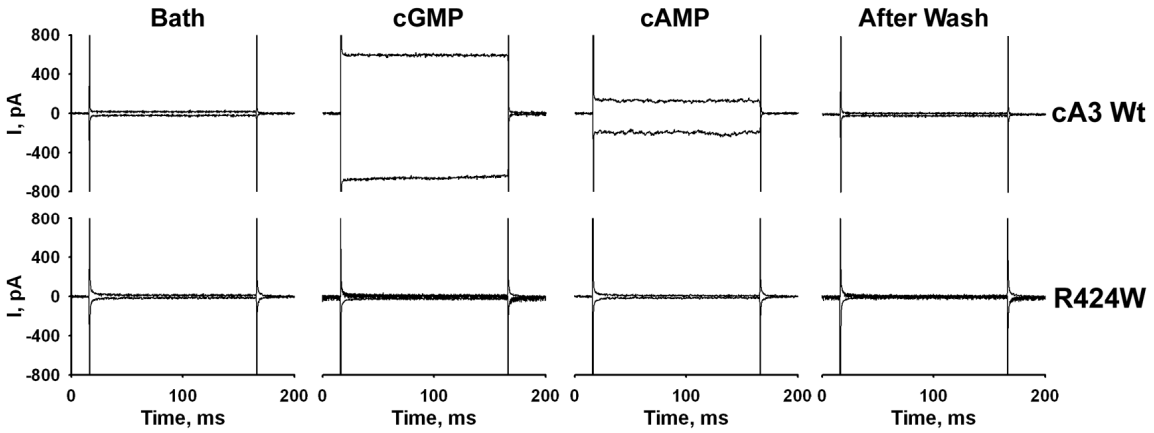

Figure 5.2 Cyclic nucleotide-activated currents in canine CNGA3 wild-type and canine CNGA3-R424W mutant channels. Excised patch clamping showed no activated currents in the mutant channels at – 60 and + 60 mV. Currents were recorded in the presence of saturating concentrations of cGMP and cAMP, 200 μM and 5000 μM respectively, at - 60 mV and 60 mV.

Table 5.2 Summary table of cyclic nucleotide-activation of cA3 wild-type and R424 mutant channels from multiple patches. c = canine.

cA3	Wt	R424W	R424K	R424E
cGMP Responses	100% (23)	0% (10)	25% (4)	0% (5)
cAMP Responses	100% (23)	0% (10)	25% (4)	0% (2)

5.3.2 Cellular localization of cA3-R424W

The localization of cA3-R424W mutant channels was examined using a YFP-tag as described in CHAPER 3.3.2. Compared to wild-type, the cA3-R424W mutation increased the number of cells with intracellular aggregates (Figure 5.3 and 5.4). Unlike the cA3-D3/N mutation that mostly resulted in mislocalization with intracellular aggregates, however, a significant fraction of cells had the wild-type phenotypes (Golgi-like and membrane fluorescence). In the expression patterns of cA3-R424W compared to those of cA3-D3/N, there is a statistically significant increase in membrane fluorescence and a significant decrease in intracellular aggregates. Along with the electrophysiological data in which the R/K mutation, conserving the positive charge, preserved some cyclic nucleotide-activated currents, the role of this Arg 424 residue might be quite different than that of the D3 residue in the S2 *Tri-Asp motif* (refer to SUMMARY for detail).

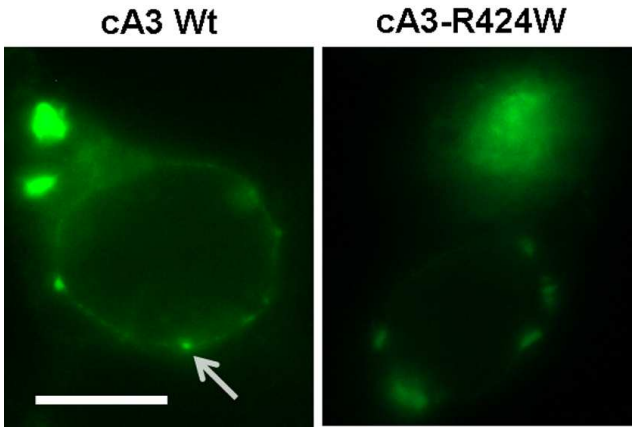

Figure 5.3 Cellular localization of YFP-tagged canine CNGA3-R424W. Cells expressing cA3-R424W can be divided into two groups. One group (the top cell in the right picture) shows intracellular aggregates. The other (the bottom cell in the right picture) shows Golge-like orgallens and membrane. The arrow indicates a Golgi-like organelle, and the scale bar is 10 μm.

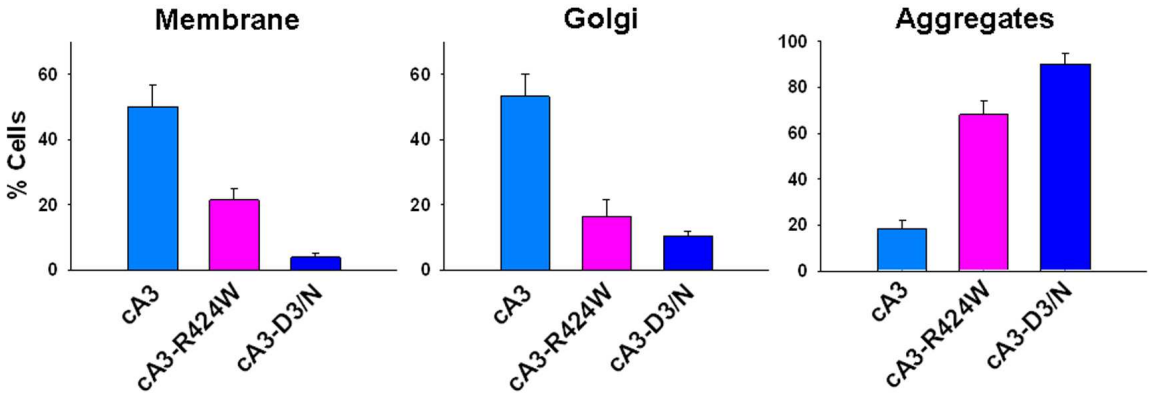

Figure 5.4 Averaged expression characteristics are shown in histograms. Histograms were constructed from counts of >200 cells. The cA3-R424W mutation expression showed an increase in intracellular aggregates, but not as much of an increase as the cA3-D3/N mutation ($p = 0.02$ on unpaired t-test). The cA3-R424W mutation showed more membrane fluorescence than the D3/N mutation.

5.3.3 Predicted interaction of Arg 424 with Glu 306 in S4-S5 linker by MD simulations

In order to investigate the molecular role of the Arg 424 residue, the Asp residue was closely examined in the cA3 homology model relaxed with MD simulations (Figure 5.5 and 5.6). The Arg 424 in the subunit P4 is interacting with the negatively charged residue, Glu 306, suggesting possible salt bridge formation. According to the homology model and the amino acid sequence alignment of Shaker K^+ superfamily members (Figure 5.7), this E306 is the very first residue of the S4 – S5 linker.

Interestingly, when looking at the amino acid sequences of Kv channels, the negatively charged residue in the S4-S5 linker and positively charged residue in S6 are reversed. In Kv channels, the first residue of the S4-S5 linker is a positively charged amino acid, Lys (K), and the last residue of S6 is a negatively charged amino acid, Glu (E). Kv channels might have an electrostatic interaction in a reversed orientation. When Arg 424 was mutated to Glu as in Kv channels (cA3-R424E), no cyclic activated-currents were observed. If there was an interaction between E306 and R424, we asked whether the double mutation of reversing these charged residues, Glu 306 to Arg and Arg 424 to Glu (*cA3-E306R-R424E*), could rescue the channel function (continued to 5.3.4).

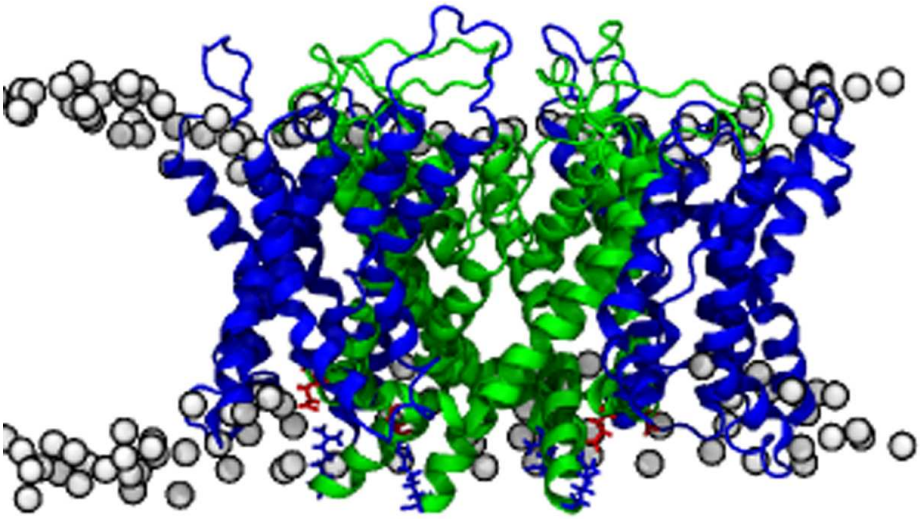

Figure 5.5 Side view of the canine CNGA3 homotetramer model in its environment. The voltage-sensing domain (S1 – S4) is presented in green, and the pore-forming region (S5 – S6) is presented in blue. The residues E306 and R424 are presented in red and blue respectively. Side chains are omitted for clarity. The phosphates of POPC lipids embedding the channel are represented as VDW spheres. Carbons, oxygens, and nitrogens of POPC lpids as well as water molecules and ions are not shown for clarity.

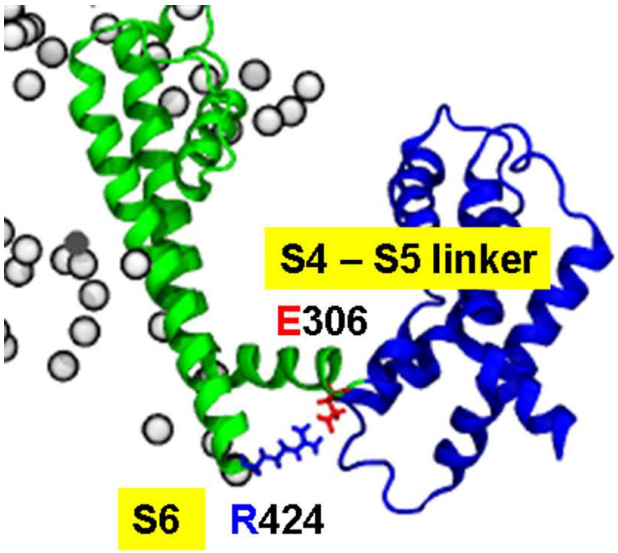

Figure 5.6 Predicted interaction between R424 in S6 and E306 in S4-S5 linker. One of the four subunits, P4, indicates that the Arg 424 (blue) forms a salt bridge with the E306 (red) in the very beginning of the S4 – S5 linker.

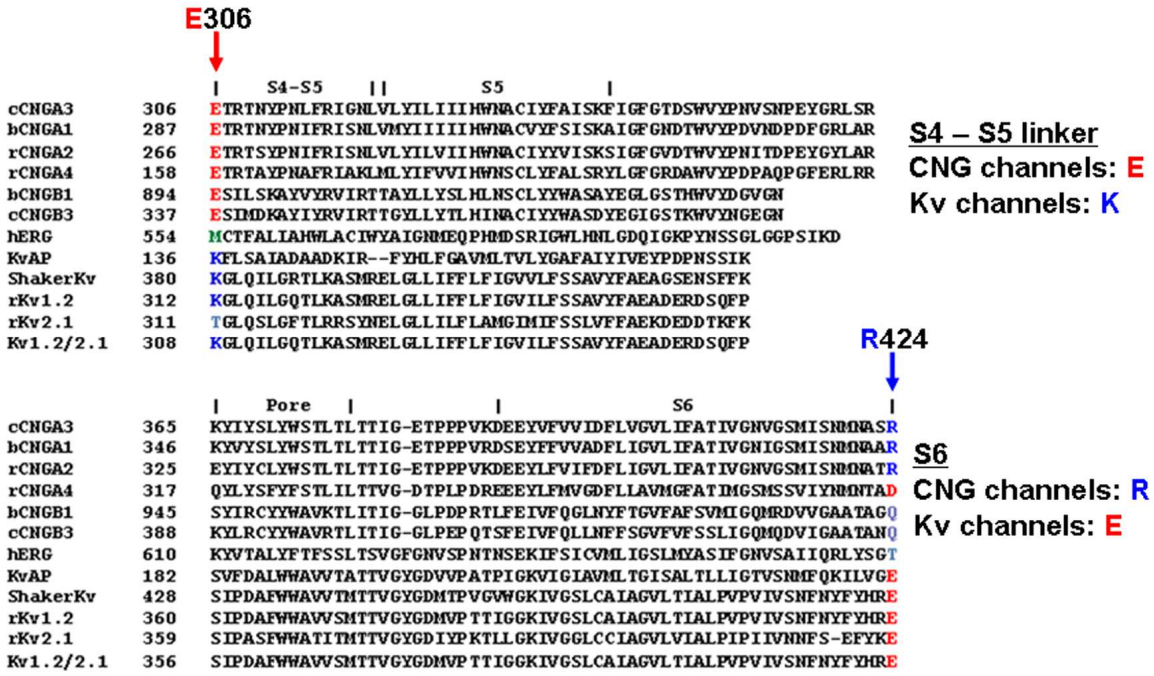

Figure 5.7 Amino acid sequence alignment of the S4-S5 linker to the S6 segment of Shaker superfamily channels. cA3-E306 is the very first residue of the S4 – S5 linker. cA3-R424 is the very last residue of S6. In Kv channels, the charges of these residues are reversed. c = canine; b = bovine; h = human; r = rat. CNGA1 and CNGB1 are rod channels; CNGA2 and CNGA4 are channel subunits expressed in olfactory cilia.

5.3.4 The double mutation, *cA3-E306R-R424E*, rescued channel function.

The construct of the double mutation, *cA3-E306R-R424E* was made as in Materials and methods. Electrophysiology data showed no cyclic nucleotide-activated currents from single mutant channel, cA3-R424E, but responsive patches from cA3-E306R-R424E channels. The reversing of the charges on these residues, conserving two opposite charges, could maintain channel function. These experimental results support the hypothesis gained from the computational study that there is an interaction between Glu 306 in the S4 – S5 linker and R424 in S6. The R424W missense mutation in the A3

subunit might disrupt this slat bridge formation and cause daylight blindness in dogs (see Summary for detail).

cA3	Wt	R424E	E306R-R424E
cGMP Responses	100% (23)	0% (4)	100% (5)
cAMP Responses	100% (23)	0% (3)	100% (2)

Table 5.3 Summary table of cyclic nucleotide-activation of cA3 wild-type, R424E, and E306R-R424E mutant channels from multiple patches. The double mutation rescued the channel function. c = canine.

5.4 Summary

5.4.1 Loss of channel function and mislocalization in cA3-R424W mutant channels

A3-R424W mutant channels resulted in no cyclic nucleotide-activated currents. Localization studies with an YFP-tag showed an increase in the number of cells with intracellular aggregates. However, the localization of cA3-R424W mutant channels also showed many cells with the proper localization of Golgi-like and membrane fluorescence, suggesting that the localization of the cA3-R424W was not altered as severely as the D3/N missense mutation in S2 *Tri-Asp motif*. In addition, electrophysiological data showed that the R424K mutation, conserving the positive charge, preserved channel function in some cells. These results differ from the results of the D3/E mutation in which the conserving of the negative charge could not maintain channel function. The Arg 424 residue might have a different molecular biochemical role than the D3 residue in the S2 *Tri-Asp motif*.

5.4.2 Salt bridge formation between Arg 424 and Glu 306 in the S4-S5 linker

In the cA3 homology model with MD simulations, one of the four subunits (P4) predicted that the Arg 424 was electrostatically interacting with the Glu 306 residue in the S4-S5 linker. Moreover, patch clamp electrophysiology revealed that the single mutation of Arg 424 to the opposite negative charge, Glu, (R424E) led to loss of cyclic nucleotide-activated currents, yet the double mutation of reversing these residues, Glu 306 to Arg and Arg 424 to Glu (E306R-R424E), could rescue channel function. Combining these computational and functional studies, therefore, a salt bridge is likely to

be formed between E306 in S4-S5 linker and R424 in S6. The cA3-R424W mutation might lead to disruption of this slat bridge formation.

CHAPTER 6

DISCUSSION

6.1 What insights emerge from my studies on the canine daylight blind D262N missense mutation in CNGB3?

6.1.1 The missense D3/N mutation in cA3 results in loss of function and mislocalization.

Loss of channel function is apparent in patches from homomeric cA3-D3/N mutant channels in which no cGMP-activated currents were seen. Cellular localization studies of cA3-D3/N channels with a YFP-tag show very few cells express membrane or Golgi fluorescence, and nearly 100% express intracellular aggregates. Other studies on achromatopsia mutations in CNG channels show similar a loss or alterations of channel function associated with defects in folding, cellular localization and/or trafficking (Ding et al., 2010; Matveev et al., 2010; Patel et al., 2005; Saliba et al., 2002). Mislocalization and loss of function are considered to be typical phenotypes of channelopathies in general (Ashcroft, 2006). Mutations in rhodopsin and hA3 have reported to cause ER stress, leading to cell death (Duricka et al., 2012; Saliba et al., 2002). Mislocalization (ER retention) might be attributed to misfolding (refer to 6.3.1).

6.1.2 When co-expressed with canine CNGA3 + human CNGB3-D3/N, there are two populations, homomeric canine CNGA3 and heteromeric canine CNGA3 + human CNGB3-D3/N channels.

1) Homomeric canine CNGA3 channel assembly is favored in the presence of the mutant D3/N-B3.

My patch currents show that ~ 20% of the cells co-transfected with cA3 + hB3 express homomeric channels. When cA3 is co-expressed with mutant hB3-D3/N subunits, ~ 60% of patches have homomeric-type currents with no evidence of functional heteromeric channels. Cellular localization studies of cA3 + hB3-D3/N reveal a mix of the normal phenotype (membrane and Golgi-like features) and the mutant phenotype (intracellular aggregates). We posit two populations of channels: functional homomeric cA3 and mis-trafficked, dysfunctional heteromeric cA3 + hB3-D3/N channels. My data suggest that misfolded B3-D3/N subunits favor the assembly of A3 homomeric channels compared to the favored assembly of heteromeric channels when wild-type B3 subunits are available. Following our hypothesis of misfolded D3/N mutants, we propose that cA3 trimers interact in 60 % of the cases with another properly folded cA3 subunit while 40% of the cases with a misfolded cB3 subunit leaded to a loss of channel function. The mechanism of heteromeric channel assembly is discussed more in detail in 6.2.

2) The CNGB3 mutant dogs might have disease because of alterations in Ca^{2+} homeostasis.

If cA3 subunits form homomeric functional channels in a heterologous expression system in the presence of a misfolded mutant B3 subunit, why is there no evidence of A3 homomeric channels in the outer segments of the daylight blind mutant dogs (Komaromy et al., 2010)? In the B3 mutant dogs, A3-only channels might be expressed, but the greatly reduced Ca^{2+} influx could lead to profound disturbances in outer segment Ca^{2+} homeostasis (Wei et al., 2012). Previous studies examining Ca^{2+} homeostasis effects in photoreceptors reported an increase of intracellular calcium concentration results in cone dystrophies and apoptotic cell death in photoreceptors (Behnen et al., 2010; Fox et al., 1999).

3) The CNGB3 subunit might be required for proper trafficking of the A3 subunit.

Another possible explanation for the absence of A3 homomeric channels in the outer segments of the daylight blind mutant dogs is that the B3 subunit might affect the trafficking of the A3 subunit. A previous study reported that hA3 subunit expression was increased in oocytes when co-expressed with hB3 (Peng et al., 2003b). My localization studies showed no significant differences between Golgi-like and membrane fluorescence of homo- and heteromeric channels, but a slight increase in intracellular aggregates with co-expression of cA3 + hB3. These *in vitro* data suggest that the B3 subunit alters the trafficking of the A3 subunit. However, A3 subunits alone form functional homomeric

channels in heterologous expression, which does not match the results from retina immunohistochemistry results in which no A3 subunit expression is seen in the outer segments of the B3 deletion mutant dogs.

6.2 What regulates subunit associations in CNG channels?

6.2.1 The stoichiometry of cone CNG channels is more ambiguous than that of rod CNG channels

The cyclic nucleotide-binding domain of CNG channels is followed by a C-leucine zipper (CLZ) region which has been shown to be involved in subunit organization. An elegant investigation of the CLZ domain of CNG channels by Zagotta and colleagues provides insights as well as deeper questions about CNG channel heteromeric assembly (Shuart et al., 2011). They examined the CLZ domain properties using intact channels as well as soluble CLZ domain constructs from both CNGA1 (A1) and A3. The soluble CLZ domains were crystallized and the structures reveal long, parallel, three-helix, coiled-coil domains. Their study supports previous models of rod CNG channel assembly and stoichiometry in which an initial A1 trimer forms followed by a high affinity association of the trimeric assembly with a CNGB1 (B1) subunit (Weitz et al., 2002; Zheng et al., 2002; Zhong et al., 2002). The assembly of cone CNG channels may not follow rigid association rules because reports show a 2:2 (Peng et al., 2004) as well as a 3:1 A3:B3 ratio (Shuart et al., 2011; Zhong et al., 2003). Although

both CLZ soluble domains (A1 and A3) form trimeric coiled-coil helices, their structures are not identical. Might these structures encrypt differences in the tetramerization interfaces altering the affinity and efficiency of the CNG channel B-type subunit recruitment? Also to be considered, olfactory CNG channels have a 2:1:1 subunit composition with CNGA2:CNGA4:CNGB1b yet both CNGA2 and CNGA4 have CLZ domains (Zheng and Zagotta, 2004).

6.2.2 The mechanism of communication between subunits for heteromeric channel assembly remains to be determined.

The CNGB1 and CNGB3 do not express CLZ domains. The proposed high-affinity molecular interface between the CLZ trimer of A1 and A3 with a B-type partner has yet to be defined although there is evidence that the N-terminal region of CNGB1 (B1) is involved in heteromeric assembly (Shuart et al., 2011; Trudeau and Zagotta, 2002a). In previous co-expression studies, Yau and collaborators co-transfected hA3 + hB1 in ratios from 25% hB1 to 5 times more hB1 (Zhong et al., 2003). Based on cAMP efficacy, nearly 100% of the currents were heteromeric. Varnum and collaborators investigated the hA3 and hB3 subunit assembly in oocytes varying the mRNA ratios 10 fold (Peng et al., 2004). Based on their cAMP efficacy and L-*cis*-diltiazem block, the current characteristics were heteromeric and independent of the mRNA ratios.

My data, however, show evidence of two populations of homomeric cA3 and heteromeric cA3 + hB3 channels when co-expressed with cA3 + hB3. Moreover, the homomeric assembly of cA3 channels is even more favored when co-transfected with the

missense B3-D3/N mutation as described in 6.1.1. These results might indicate that heteromeric subunit assembly is less efficient with subunits from different species. The lack of a suitable cB3 gene for heterologous expression studies as well as for canine gene therapy prompted the substitution of the hB3 in treatment studies (Garcia et al., 2010; Komaromy et al., 2010). Thus, the functional channels expressed in the treated mutant dog should have the same subunit composition as the heteromeric channels studied here. The effect of gene replacement therapy on daylight blind dogs using the *hB3* gene has lasted for up to two years (Komaromy et al., 2010), yet would the effect last longer if the *cB3* gene were cloned and used? Would the heteromeric channel assembly be more favored in heterologous expression if co-expressed with A-type and B-type subunits from the same species? In the differences between the sequences of canine and human B3 subunits, is there any particular region which would read information about the species differences? Future studies might define the molecular interactions involved at the subunit interfaces in heteromeric channel assembly.

6.3 What insights about the *Tri-Asp motif* emerge from my studies?

6.3.1 All the Asp mutations of the *Tri-Asp motif* result in loss of channel function and mislocalization

Despite trying all the different substitutions with non-polar, polar, and charged residues, none of the Asp mutations in the *Tri-Asp motif* exhibited cyclic nucleotide-

activated currents or proper trafficking. Nor did any of the D/E substitutions, conserving the negative charge, preserve channel function. In our homology model of the cA3 channel with MD simulations, however, the Asp residues of the *Tri-Asp motif* are involved in global electrostatic salt bridge networking formed by unspecific parings. Given that the pairings of negative and positive charged residues are unspecific and that the network is global, it is unlikely that one single amino acid change could completely destroy channel structure and function, much less the D/E substitution. That leaves us with the question of what is the role of these acidic residues? (Continued to 6.3.2)

6.3.2 Proper bundle forming with the *Tri-Asp* residues and other charged residues in S2 – S4 might be critical for threading into the membrane during CNG channel biogenesis

In Shaker, the interaction between charged residues of S2 – S4 is important to stabilize helices S2 – S4 that span the membrane (Papazian et al., 1995; Planells-Cases et al., 1995; Silverman et al., 2003; Wu et al., 2010). A similar mechanism was reported in Na^+ selective channels of the same six transmembrane segment family (Decaen et al., 2009). Furthermore, recently, electrostatic interactions between the residue in the position of D3 and the positive residues of S4 have been shown to mediate folding and membrane insertion in both the plant Kv-like channel KAT1 and in Shaker (Sato et al., 2002; Sato et al., 2003; Zhang et al., 2007). In the folding model for Shaker channels inferred from these studies, folding of this region involves a two step mechanism: the uncharged helix S1 is inserted first in the membrane. Charged amino acids from S2 – S3

– S4 are then paired to form a three helix bundle and this assembly is released from the translocon into the membrane.

All the *Tri-Asp* mutant channels resulted in loss of channel function and mislocalization, suggesting that the *Tri-Asp motif* in CNG channels is critical for folding, assembly, trafficking, and/or function. Furthermore, my experiments involving D/E mutations showed that not only charge conservation is important, but also residue length. The previous work cited above on Shaker folding reached the same conclusion (Zhang et al., 2007). Unlike for function conservation where the charge preservation may be enough, during protein folding, on the other hand, a conserved negative charge might not be enough and strict conservation of Asp might be required. Considering the sequence and structural similarity between Shaker superfamily members, we thus propose that mutation of D3 or any *Tri-Asp* residue to any other amino acid would likely lead to protein misfolding.

6.4 What insights emerge from my studies on the canine daylight blind missense R424 mutation in CNGA3?

6.4.1 The canine *CNGA3-R424W* mutation results in loss of function, but not as severe mislocalization as the D3/N mutation

A3-R424W mutant channels resulted in no cyclic nucleotide-activated currents and mislocalization with intracellular aggregates. These results show similar phenotypes

to what has been reported in other achromatopsia mutation studies (Ding et al., 2010; Matveev et al., 2010; Patel et al., 2005; Saliba et al., 2002). However, the localization of cA3-R424W mutant channels was not affected as severely as the D3/N missense mutation in S2 *Tri-Asp motif*, showing a lot of cells with the proper localization of Golgi-like and membrane fluorescence. Moreover, the R424K mutation, conserving the positive charge, preserved channel function in some cells, which is different from the results in which the D3/E mutation, conserving the negative charge, led to loss of cyclic nucleotide-activated currents. Even though these missense mutations are both associated with canine daylight blindness, electrophysiology and localization studies suggest that the molecular biochemical roles of these two residues might not be quite the same. The Arg 424 residue might not be as critical for folding as the D3 residue in the S2 *Tri-Asp motif*. The effect of the R424E mutation might be more of a problem in channel structure and function (continued to 6.4.2).

6.4.2 The Arg 424 residue in S6 might form a salt bridge with the Glu 304 residue in the S4-S5 linker to maintain the pore-forming region open.

The cA3 model relaxed with MD simulations indicated a possible interaction of Arg 424 with the Glu 304 residue in the S4-S5 linker. This hypothesis is supported by electrophysiological data. The single mutation of Arg 424 to Glu (R424E) result in loss of cyclic nucleotide-activated currents, yet the double mutation of reversing these residues, Glu 306 to Arg and Arg 424 to Glu (E306R-R424E) preserves channel function. In the model, this salt bridge appears to contribute to stabilization of the open

pore state. The R424W mutation might disrupt the salt bridge formation, leading to deforming and closing the pore region. The cA3-R424W missense mutant model with MD simulations is underway to gain more insights about the electrostatic interaction and the open state of the channel. Furthermore, since Kv channels share the same pattern of charged residues at these positions in a reversed way, it would be worth while to determine whether this salt bridge would form in related Kv channels for the open state confirmation.

REFERENCES

Abernethy,D.R. and J.B.Schwartz. 1999. Calcium-antagonist drugs. *N. Engl. J. Med.* 341:1447-1457.

Aligianis,I.A., T.Forshew, S.Johnson, M.Michaelides, C.A.Johnson, R.C.Trembath, D.M.Hunt, A.T.Moore, and E.R.Maher. 2002. Mapping of a novel locus for achromatopsia (ACHM4) to 1p and identification of a germline mutation in the alpha subunit of cone transducin (GNAT2). *J Med. Genet.* 39:656-660.

Altschul,S.F., W.Gish, W.Miller, E.W.Myers, and D.J.Lipman. 1990. Basic local alignment search tool. *J Mol Biol* 215:403-410.

Ashcroft,F.M. 2006. From molecule to malady. *Nature* 440:440-447.

Behnen,P., D.Dell'Orco, and K.W.Koch. 2010. Involvement of the calcium sensor GCAP1 in hereditary cone dystrophies. *Biol Chem* 391:631-637.

Biel,M. and S.Michalakis. 2009. Cyclic nucleotide-gated channels. *Handb. Exp. Pharmacol.*:111-136.

Brelidze,T.I., A.E.Carlson, B.Sankaran, and W.N.Zagotta. 2012. Structure of the carboxy-terminal region of a KCNH channel. *Nature* 481:530-533.

Clayton,G.M., S.Altieri, L.Heginbotham, V.M.Unger, and J.H.Morais-Cabral. 2008. Structure of the transmembrane regions of a bacterial cyclic nucleotide-regulated channel. *Proc. Natl. Acad. Sci. U. S. A* 105:1511-1515.

Darden,T., D.York, and L.Pedersen. 1993. Particle Mesh Ewald - An N.Log(N) Method for Ewald Sums in Large Systems. *Journal of Chemical Physics* 98:10089-10092.

Decaen,P.G., V.Yarov-Yarovoy, E.M.Sharp, T.Scheuer, and W.A.Catterall. 2009. Sequential formation of ion pairs during activation of a sodium channel voltage sensor. *Proc Natl Acad Sci U. S. A* 106:22498-22503.

Ding,X.Q., J.B.Fitzgerald, A.B.Quiambao, C.S.Harry, and A.P.Malykhina. 2010. Molecular pathogenesis of achromatopsia associated with mutations in the cone

cyclic nucleotide-gated channel CNGA3 subunit. *Adv. Exp Med Biol* 664:245-253.

Doyle,D.A., C.J.Morais, R.A.Pfuetzner, A.Kuo, J.M.Gulbis, S.L.Cohen, B.T.Chait, and R.MacKinnon. 1998. The structure of the potassium channel: molecular basis of K+ conduction and selectivity. *Science* 280:69-77.

Duricka,D.L., R.L.Brown, and M.D.Varnum. 2012. Defective trafficking of cone photoreceptor CNG channels induces the unfolded protein response and ER-stress-associated cell death. *Biochem. J.* 441:685-696.

Eswar,N., B.Webb, M.A.Marti-Renom, M.S.Madhusudhan, D.Eramian, M.Y.Shen, U.Pieper, and A.Sali. 2006. Comparative protein structure modeling using Modeller. *Curr. Protoc. Bioinformatics.* Chapter 5:Unit.

Fox,D.A., A.T.Poblenz, and L.He. 1999. Calcium overload triggers rod photoreceptor apoptotic cell death in chemical-induced and inherited retinal degenerations. *Ann. N. Y. Acad Sci* 893:282-285.

Frings,S., R.Seifert, M.Godde, and U.B.Kaupp. 1995. Profoundly different calcium permeation and blockage determine the specific function of distinct cyclic nucleotide-gated channels. *Neuron* 15:169-179.

Garcia,M.M., G.S.Ying, C.A.Cocores, J.C.Tanaka, and A.M.Komaromy. 2010. Evaluation of a behavioral method for objective vision testing and identification of achromatopsia in dogs. *Am. J Vet. Res.* 71:97-102.

Gosselin-Badaroudine,P., L.Delemotte, A.Moreau, M.L.Klein, and M.Chahine. 2012. Gating pore currents and the resting state of Nav1.4 voltage sensor domains. *Proc Natl Acad Sci U. S. A* 109:19250-19255.

Grunwald,M.E., W.P.Yu, H.H.Yu, and K.W.Yau. 1998. Identification of a domain on the beta-subunit of the rod cGMP-gated cation channel that mediates inhibition by calcium-calmodulin. *J Biol. Chem.* 273:9148-9157.

Haynes,L. and K.W.Yau. 1985. Cyclic GMP-sensitive conductance in outer segment membrane of catfish cones. *Nature* 317:61-64.

Haynes,L.W. 1995. Permeation and block by internal and external divalent cations of the catfish cone photoreceptor cGMP-gated channel. *J Gen. Physiol* 106:507-523.

Haynes,L.W. and K.W.Yau. 1990. Single-channel measurement from the cyclic GMP-activated conductance of catfish retinal cones. *J Physiol* 429:451-481.

Izaguirre,J.A., S.Reich, and R.D.Skeel. 1999. Longer time steps for molecular dynamics. *Journal of Chemical Physics* 110:9853-9864.

Jorgensen,W.L., J.Chandrasekhar, J.D.Madura, R.W.Impey, and M.L.Klein. 1983. Comparison of Simple Potential Functions for Simulating Liquid Water. *Journal of Chemical Physics* 79:926-935.

Kaupp,U.B., T.Niidome, T.Tanabe, S.Terada, W.Bonigk, W.Stuhmer, N.J.Cook, K.Kangawa, H.Matsuo, T.Hirose, and . 1989. Primary structure and functional expression from complementary DNA of the rod photoreceptor cyclic GMP-gated channel. *Nature* 342:762-766.

Kaupp,U.B. and R.Seifert. 2002. Cyclic nucleotide-gated ion channels. *Physiol Rev.* 82:769-824.

Koeppen,K., P.Reuter, S.Kohl, B.Baumann, T.Ladewig, and B.Wissinger. 2008. Functional analysis of human CNGA3 mutations associated with colour blindness suggests impaired surface expression of channel mutants A3(R427C) and A3(R563C). *Eur. J Neurosci.* 27:2391-2401.

Kohl,S., B.Baumann, M.Broghammer, H.Jagle, P.Sieving, U.Kellner, R.Spegal, M.Anastasi, E.Zrenner, L.T.Sharpe, and B.Wissinger. 2000. Mutations in the CNGB3 gene encoding the beta-subunit of the cone photoreceptor cGMP-gated channel are responsible for achromatopsia (ACHM3) linked to chromosome 8q21. *Hum. Mol. Genet.* 9:2107-2116.

Kohl,S., B.Baumann, T.Rosenberg, U.Kellner, B.Lorenz, M.Vadala, S.G.Jacobson, and B.Wissinger. 2002. Mutations in the cone photoreceptor G-protein alpha-subunit gene GNAT2 in patients with achromatopsia. *Am. J Hum. Genet.* 71:422-425.

Kohl,S., H.Jagle, and B.Wissinger. 1993. Achromatopsia.

Kohl,S., T.Marx, I.Giddings, H.Jagle, S.G.Jacobson, E.Apfelstedt-Sylla, E.Zrenner, L.T.Sharpe, and B.Wissinger. 1998. Total colourblindness is caused by mutations in the gene encoding the alpha-subunit of the cone photoreceptor cGMP-gated cation channel. *Nat. Genet* 19:257-259.

Komaromy,A.M., J.J.Alexander, J.S.Rowlan, M.M.Garcia, V.A.Chiodo, A.Kaya, J.C.Tanaka, G.M.Acland, W.W.Hauswirth, and G.D.Aguirre. 2010. Gene therapy rescues cone function in congenital achromatopsia. *Hum. Mol. Genet.* 19:2581-2593.

Korenbrot,J.I. 1995. Ca2+ flux in retinal rod and cone outer segments: differences in Ca2+ selectivity of the cGMP-gated ion channels and Ca2+ clearance rates. *Cell Calcium* 18:285-300.

Korenbrot,J.I. 2012. Speed, sensitivity, and stability of the light response in rod and cone photoreceptors: facts and models. *Prog. Retin. Eye Res.* 31:442-466.

Korschen,H.G., M.Illing, R.Seifert, F.Sesti, A.Williams, S.Gotzes, C.Colville, F.Muller, A.Dose, M.Godde, and . 1995. A 240 kDa protein represents the complete beta subunit of the cyclic nucleotide-gated channel from rod photoreceptor. *Neuron* 15:627-636.

Kraus-Friedmann,N. 2000. Cyclic nucleotide-gated channels in non-sensory organs. *Cell Calcium* 27:127-138.

Larkin,M.A., G.Blackshields, N.P.Brown, R.Chenna, P.A.McGettigan, H.McWilliam, F.Valentin, I.M.Wallace, A.Wilm, R.Lopez, J.D.Thompson, T.J.Gibson, and D.G.Higgins. 2007. Clustal W and Clustal X version 2.0. *Bioinformatics.* 23:2947-2948.

Lee,S.Y., A.Lee, J.Chen, and R.MacKinnon. 2005. Structure of the KvAP voltage-dependent K+ channel and its dependence on the lipid membrane. *Proc. Natl. Acad. Sci. U. S. A* 102:15441-15446.

Levine,M., S.C.Curry, A.Padilla-Jones, and A.M.Ruha. 2013. Critical care management of verapamil and diltiazem overdose with a focus on vasopressors: a 25-year experience at a single center. *Ann. Emerg. Med.* 62:252-258.

Lewis,C.A. 1979. Ion-concentration dependence of the reversal potential and the single channel conductance of ion channels at the frog neuromuscular junction. *J Physiol* 286:417-445.

Lindahl,E.R. 2008. Molecular dynamics simulations. *Methods Mol. Biol.* 443:3-23.

Liu,C., T.Sherpa, and M.D.Varnum. 2013. Disease-associated mutations in CNGB3 promote cytotoxicity in photoreceptor-derived cells. *Mol. Vis.* 19:1268-1281.

Long,S.B., X.Tao, E.B.Campbell, and R.MacKinnon. 2007. Atomic structure of a voltage-dependent K+ channel in a lipid membrane-like environment. *Nature* 450:376-382.

MacKerell,A.D., D.Bashford, M.Bellott, R.L.Dunbrack, J.D.Evanseck, M.J.Field, S.Fischer, J.Gao, H.Guo, S.Ha, D.Joseph-McCarthy, L.Kuchnir, K.Kuczera, F.T.K.Lau, C.Mattos, S.Michnick, T.Ngo, D.T.Nguyen, B.Prodhom, W.E.Reiher, B.Roux, M.Schlenkrich, J.C.Smith, R.Stote, J.Straub, M.Watanabe, J.Wiorkiewicz-Kuczera, D.Yin, and M.Karplus. 1998. All-atom empirical potential for molecular modeling and dynamics studies of proteins. *Journal of Physical Chemistry B* 102:3586-3616.

MacKerell,A.D., M.Feig, and C.L.Brooks. 2004. Extending the treatment of backbone energetics in protein force fields: Limitations of gas-phase quantum mechanics in reproducing protein conformational distributions in molecular dynamics simulations. *Journal of Computational Chemistry* 25:1400-1415.

Matveev,A.V., J.B.Fitzgerald, J.Xu, A.P.Malykhina, K.K.Rodgers, and X.Q.Ding. 2010. The disease-causing mutations in the carboxyl terminus of the cone cyclic nucleotide-gated channel CNGA3 subunit alter the local secondary structure and interfere with the channel active conformational change. *Biochemistry* 49:1628-1639.

Muraki-Oda,S., F.Toyoda, A.Okada, S.Tanabe, S.Yamade, H.Ueyama, H.Matsuura, and M.Ohji. 2007. Functional analysis of rod monochromacy-associated missense mutations in the CNGA3 subunit of the cone photoreceptor cGMP-gated channel. *Biochem. Biophys. Res. Commun.* 362:88-93.

Nakajima,T., T.Furukawa, T.Tanaka, Y.Katayama, R.Nagai, Y.Nakamura, and M.Hiraoka. 1998. Novel mechanism of HERG current suppression in LQT2: shift in voltage dependence of HERG inactivation. *Circ. Res.* 83:415-422.

O'Sullivan,B.P. and S.D.Freedman. 2009. Cystic fibrosis. *Lancet* 373:1891-1904.

Okada,A., H.Ueyama, F.Toyoda, S.Oda, W.G.Ding, S.Tanabe, S.Yamade, H.Matsuura, I.Ohkubo, and K.Kani. 2004. Functional role of hCNGB3 in regulation of human cone cng channel: effect of rod monochromacy-associated mutations in hCNGB3 on channel function. *Invest Ophthalmol. Vis. Sci* 45:2324-2332.

Ouechtati,F., A.Merdassi, Y.Bouyacoub, L.Largueche, K.Derouiche, H.Ouragini, S.Nouira, L.Tiab, K.Baklouti, A.Rebai, D.F.Schorderet, F.L.Munier, L.Zografos, S.Abdelhak, and M.L.El. 2011. Clinical and genetic investigation of a large Tunisian family with complete achromatopsia: identification of a new nonsense mutation in GNAT2 gene. *J Hum. Genet.* 56:22-28.

Paillart,C., K.Zhang, T.I.Rebrik, W.Baehr, and J.I.Korenbrot. 2006. Cloning and molecular characterization of cGMP-gated ion channels from rod and cone photoreceptors of striped bass (M. saxatilis) retina. *Vis. Neurosci.* 23:99-113.

Papazian,D.M., X.M.Shao, S.A.Seoh, A.F.Mock, Y.Huang, and D.H.Wainstock. 1995. Electrostatic interactions of S4 voltage sensor in Shaker K+ channel. *Neuron* 14:1293-1301.

Parrinello,M. and A.Rahman. 1980. Crystal-Structure and Pair Potentials - A Molecular-Dynamics Study. *Physical Review Letters* 45:1196-1199.

Patel,K.A., K.M.Bartoli, R.A.Fandino, A.N.Ngatchou, G.Woch, J.Carey, and J.C.Tanaka. 2005. Transmembrane S1 mutations in CNGA3 from achromatopsia 2 patients cause loss of function and impaired cellular trafficking of the cone CNG channel. *Invest Ophthalmol. Vis. Sci* 46:2282-2290.

Peng,C., E.D.Rich, C.A.Thor, and M.D.Varnum. 2003a. Functionally important calmodulin-binding sites in both NH2- and COOH-terminal regions of the cone photoreceptor cyclic nucleotide-gated channel CNGB3 subunit. *J Biol Chem* 278:24617-24623.

Peng,C., E.D.Rich, and M.D.Varnum. 2003b. Achromatopsia-associated mutation in the human cone photoreceptor cyclic nucleotide-gated channel CNGB3 subunit alters the ligand sensitivity and pore properties of heteromeric channels. *J Biol Chem* 278:34533-34540.

Peng,C., E.D.Rich, and M.D.Varnum. 2004. Subunit configuration of heteromeric cone cyclic nucleotide-gated channels. *Neuron* 42:401-410.

Phillips,J.C., R.Braun, W.Wang, J.Gumbart, E.Tajkhorshid, E.Villa, C.Chipot, R.D.Skeel, L.Kale, and K.Schulten. 2005. Scalable molecular dynamics with NAMD. *J Comput. Chem* 26:1781-1802.

Planells-Cases,R., A.V.Ferrer-Montiel, C.D.Patten, and M.Montal. 1995. Mutation of conserved negatively charged residues in the S2 and S3 transmembrane segments of a mammalian K+ channel selectively modulates channel gating. *Proc Natl Acad Sci U. S. A* 92:9422-9426.

Pless,S.A., J.D.Galpin, A.P.Niciforovic, and C.A.Ahern. 2011. Contributions of counter-charge in a potassium channel voltage-sensor domain. *Nat. Chem Biol* 7:617-623.

Reuter,P., K.Koeppen, T.Ladewig, S.Kohl, B.Baumann, and B.Wissinger. 2008. Mutations in CNGA3 impair trafficking or function of cone cyclic nucleotide-gated channels, resulting in achromatopsia. *Hum. Mutat.* 29:1228-1236.

Richards,M.J. and S.E.Gordon. 2000. Cooperativity and cooperation in cyclic nucleotide-gated ion channels. *Biochemistry* 39:14003-14011.

Saliba,R.S., P.M.Munro, P.J.Luthert, and M.E.Cheetham. 2002. The cellular fate of mutant rhodopsin: quality control, degradation and aggresome formation. *J Cell Sci* 115:2907-2918.

Sato,Y., M.Sakaguchi, S.Goshima, T.Nakamura, and N.Uozumi. 2002. Integration of Shaker-type K+ channel, KAT1, into the endoplasmic reticulum membrane: synergistic insertion of voltage-sensing segments, S3-S4, and independent insertion of pore-forming segments, S5-P-S6. *Proc Natl Acad Sci U. S. A* 99:60-65.

Sato,Y., M.Sakaguchi, S.Goshima, T.Nakamura, and N.Uozumi. 2003. Molecular dissection of the contribution of negatively and positively charged residues in S2, S3, and S4 to the final membrane topology of the voltage sensor in the K+ channel, KAT1. *J Biol Chem* 278:13227-13234.

Seoh,S.A., D.Sigg, D.M.Papazian, and F.Bezanilla. 1996. Voltage-sensing residues in the S2 and S4 segments of the Shaker K+ channel. *Neuron* 16:1159-1167.

Shuart,N.G., Y.Haitin, S.S.Camp, K.D.Black, and W.N.Zagotta. 2011. Molecular mechanism for 3:1 subunit stoichiometry of rod cyclic nucleotide-gated ion channels. *Nat. Commun.* 2:457.

Sidjanin,D.J., J.K.Lowe, J.L.McElwee, B.S.Milne, T.M.Phippen, D.R.Sargan, G.D.Aguirre, G.M.Acland, and E.A.Ostrander. 2002. Canine CNGB3 mutations establish cone degeneration as orthologous to the human achromatopsia locus ACHM3. *Hum. Mol. Genet.* 11:1823-1833.

Silverman,W.R., B.Roux, and D.M.Papazian. 2003. Structural basis of two-stage voltage-dependent activation in K+ channels. *Proc Natl Acad Sci U. S. A* 100:2935-2940.

Sundin,O.H., J.M.Yang, Y.Li, D.Zhu, J.N.Hurd, T.N.Mitchell, E.D.Silva, and I.H.Maumenee. 2000. Genetic basis of total colourblindness among the Pingelapese islanders. *Nat. Genet* 25:289-293.

Thiadens,A.A., N.W.Slingerland, S.Roosing, M.J.van Schooneveld, J.J.van Lith-Verhoeven, N.van Moll-Ramirez, L.I.van den Born, C.B.Hoyng, F.P.Cremers, and C.C.Klaver. 2009. Genetic etiology and clinical consequences of complete and incomplete achromatopsia. *Ophthalmology* 116:1984-1989.

Trudeau,M.C. and W.N.Zagotta. 2002a. An intersubunit interaction regulates trafficking of rod cyclic nucleotide-gated channels and is disrupted in an inherited form of blindness. *Neuron* 34:197-207.

Trudeau,M.C. and W.N.Zagotta. 2002b. Mechanism of calcium/calmodulin inhibition of rod cyclic nucleotide-gated channels. *Proc. Natl. Acad. Sci U. S. A* 99:8424-8429.

Trudeau,M.C. and W.N.Zagotta. 2003. Calcium/calmodulin modulation of olfactory and rod cyclic nucleotide-gated ion channels. *J Biol. Chem.* 278:18705-18708.

Wei,T., T.Schubert, F.Paquet-Durand, N.Tanimoto, L.Chang, K.Koeppen, T.Ott, O.Griesbeck, M.W.Seeliger, T.Euler, and B.Wissinger. 2012. Light-driven calcium signals in mouse cone photoreceptors. *J Neurosci.* 32:6981-6994.

Weitz,D., N.Ficek, E.Kremmer, P.J.Bauer, and U.B.Kaupp. 2002. Subunit stoichiometry of the CNG channel of rod photoreceptors. *Neuron* 36:881-889.

Wells,G.B. and J.C.Tanaka. 1997. Ion selectivity predictions from a two-site permeation model for the cyclic nucleotide-gated channel of retinal rod cells. *Biophys J* 72:127-140.

Wissinger,B., D.Gamer, H.Jagle, R.Giorda, T.Marx, S.Mayer, S.Tippmann, M.Broghammer, B.Jurklies, T.Rosenberg, S.G.Jacobson, E.C.Sener, S.Tatlipinar, C.B.Hoyng, C.Castellan, P.Bitoun, S.Andreasson, G.Rudolph, U.Kellner, B.Lorenz, G.Wolff, C.Verellen-Dumoulin, M.Schwartz, F.P.Cremers, E.Apfelstedt-Sylla, E.Zrenner, R.Salati, L.T.Sharpe, and S.Kohl. 2001. CNGA3 mutations in hereditary cone photoreceptor disorders. *Am. J. Hum. Genet.* 69:722-737.

Wu,D., K.Delaloye, M.A.Zaydman, A.Nekouzadeh, Y.Rudy, and J.Cui. 2010. State-dependent electrostatic interactions of S4 arginines with E1 in S2 during Kv7.1 activation. *J Gen. Physiol* 135:595-606.

Xu,J., L.Morris, A.Thapa, H.Ma, S.Michalakis, M.Biel, W.Baehr, I.V.Peshenko, A.M.Dizhoor, and X.Q.Ding. 2013. cGMP Accumulation Causes Photoreceptor Degeneration in CNG Channel Deficiency: Evidence of cGMP Cytotoxicity Independently of Enhanced CNG Channel Function. *J Neurosci.* 33:14939-14948.

Yau,K.W. and R.C.Hardie. 2009. Phototransduction motifs and variations. *Cell* 139:246-264.

Yu,F.H., V.Yarov-Yarovoy, G.A.Gutman, and W.A.Catterall. 2005. Overview of molecular relationships in the voltage-gated ion channel superfamily. *Pharmacol. Rev.* 57:387-395.

Zhang,L., Y.Sato, T.Hessa, H.G.von, J.K.Lee, I.Kodama, M.Sakaguchi, and N.Uozumi. 2007. Contribution of hydrophobic and electrostatic interactions to the membrane integration of the Shaker K+ channel voltage sensor domain. *Proc Natl Acad Sci U. S. A* 104:8263-8268.

Zhang,M., J.Liu, M.Jiang, D.M.Wu, K.Sonawane, H.R.Guy, and G.N.Tseng. 2005. Interactions between charged residues in the transmembrane segments of the voltage-sensing domain in the hERG channel. *J Membr. Biol* 207:169-181.

Zheng,J., M.C.Trudeau, and W.N.Zagotta. 2002. Rod cyclic nucleotide-gated channels have a stoichiometry of three CNGA1 subunits and one CNGB1 subunit. *Neuron* 36:891-896.

Zheng,J. and W.N.Zagotta. 2004. Stoichiometry and assembly of olfactory cyclic nucleotide-gated channels. *Neuron* 42:411-421.

Zhong,H., J.Lai, and K.W.Yau. 2003. Selective heteromeric assembly of cyclic nucleotide-gated channels. *Proc. Natl. Acad. Sci U. S. A* 100:5509-5513.

Zhong,H., L.L.Molday, R.S.Molday, and K.W.Yau. 2002. The heteromeric cyclic nucleotide-gated channel adopts a 3A:1B stoichiometry. *Nature* 420:193-198.

Zong,X., H.Zucker, F.Hofmann, and M.Biel. 1998. Three amino acids in the C-linker are major determinants of gating in cyclic nucleotide-gated channels. *EMBO J* 17:353-362.

[i] Abbreviations: CNG, cyclic nucleotide-gated; A3, CNGA3; B3, CNGB3, A3 + B3, heteromeric CNG channels formed from CNGA3 and CNGB3 subunits; S1-S6, transmembrane spanning helical regions 1-6; A3-D3/N, canine CNGA3-D231N mutant CNG channel; B3-D3/N, human CNGB3-D267N mutant CNG channel;